

CrossMark
click for updates

Research

Cite this article: Rose C, Polissar PJ, Tierney JE, Filley T, deMenocal PB. 2016 Changes in northeast African hydrology and vegetation associated with Pliocene–Pleistocene sapropel cycles. *Phil. Trans. R. Soc. B* **371**: 20150243. <http://dx.doi.org/10.1098/rstb.2015.0243>

Accepted: 22 April 2016

One contribution of 17 to a discussion meeting issue ‘Major transitions in human evolution’.

Subject Areas:

environmental science

Keywords:

Mediterranean Sea, sapropel, leaf wax, carbon isotope, hydrogen isotope, East Africa

Author for correspondence:

Peter B. deMenocal

e-mail: peter@ldeo.columbia.edu

We wish to dedicate this paper to Richard Leakey to honour his 70th birthday and in acknowledgement of his many decades of contributions to the field of human evolution.

Changes in northeast African hydrology and vegetation associated with Pliocene–Pleistocene sapropel cycles

Cassandra Rose¹, Pratigya J. Polissar², Jessica E. Tierney³, Timothy Filley⁴ and Peter B. deMenocal^{1,2}¹Department of Earth and Environmental Sciences, Columbia University, New York, NY 10027, USA²Lamont-Doherty Earth Observatory of Columbia University, Palisades, NY 10964, USA³Department of Geosciences, University of Arizona, Tucson, AZ 85721, USA⁴Department of Earth and Atmospheric Sciences, The Purdue Climate Change Research Center, Purdue University, West Lafayette, IN 47907, USA

ID PBdM, 0000-0002-7191-717X

East African climate change since the Late Miocene consisted of persistent shorter-term, orbital-scale wet–dry cycles superimposed upon a long-term trend towards more open, grassy landscapes. Either or both of these modes of palaeoclimate variability may have influenced East African mammalian evolution, yet the interrelationship between these secular and orbital palaeoclimate signals remains poorly understood. Here, we explore whether the long-term secular climate change was also accompanied by significant changes at the orbital-scale. We develop northeast African hydroclimate and vegetation proxy data for two 100 kyr-duration windows near 3.05 and 1.75 Ma at ODP Site 967 in the eastern Mediterranean basin, where sedimentation is dominated by eastern Sahara dust input and Nile River run-off. These two windows were selected because they have comparable orbital configurations and bracket an important increase in East African C₄ grasslands. We conducted high-resolution (2.5 kyr sampling) multiproxy biomarker, H- and C-isotopic analyses of plant waxes and lignin phenols to document orbital-scale changes in hydrology, vegetation and woody cover for these two intervals. Both intervals are dominated by large-amplitude, precession-scale (approx. 20 kyr) changes in northeast African vegetation and rainfall/run-off. The $\delta^{13}\text{C}_{\text{wax}}$ values and lignin phenol composition record a variable but consistently C₄ grass-dominated ecosystem for both intervals (50–80% C₄). Precessional $\delta\text{D}_{\text{wax}}$ cycles were approximately 20–30‰ in peak-to-peak amplitude, comparable with other $\delta\text{D}_{\text{wax}}$ records of the Early Holocene African Humid Period. There were no significant differences in the means or variances of the $\delta\text{D}_{\text{wax}}$ or $\delta^{13}\text{C}_{\text{wax}}$ data for the 3.05 and 1.75 Ma intervals studied, suggesting that the palaeohydrology and palaeovegetation responses to precessional forcing were similar for these two periods. Data for these two windows suggest that the eastern Sahara did not experience the significant increase in C₄ vegetation that has been observed in East Africa over this time period. This observation would be consistent with a proposed mechanism whereby East African precipitation is reduced, and drier conditions established, in response to the emergence of modern zonal sea surface temperature gradients in the tropical oceans between 3 and 2 Ma.

This article is part of the themed issue ‘Major transitions in human evolution’.

1. Introduction

The possible role of Pliocene–Pleistocene changes in East African rainfall and vegetation in shaping faunal change and hominin evolution remains a vigorous area of multidisciplinary research [1–9]. Diverse palaeovegetation proxy records from marine and terrestrial archives document an initial Late Miocene expansion

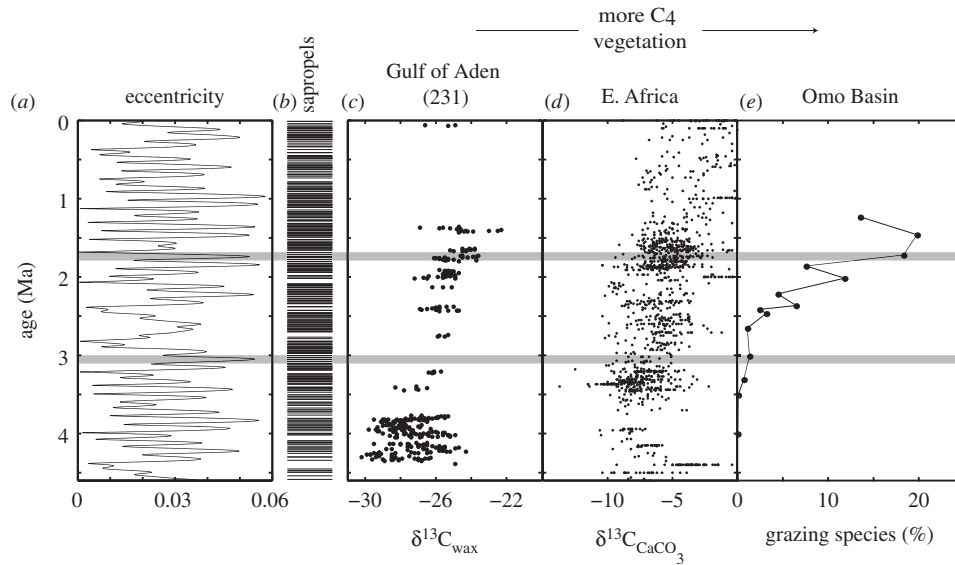


Figure 1. A comparison of East African and Mediterranean palaeoclimate records. Shaded bars indicate the periods analysed in this study. (a) Eccentricity cycles [20]. (b) Mediterranean sapropel (black lines)/carbonate cycles compiled from marine and terrestrial sections [21,22]. (c) Carbon isotope values from plant wax biomarkers from Site 231, Gulf of Aden [12]. (d) Northeast African soil carbonate carbon isotopes [2]. (e) Relative abundance of arid grassland-adapted mammals [1].

of open grassland landscapes, followed by a gradual trend towards increasingly open, C_4 -rich vegetation until 1–2 Ma, after which the modern savannah grassland expanses were established [2,9–12]. Superimposed on this secular vegetation shift were large-amplitude orbital-scale (approx. 20 ka) variations in North and East African climate and vegetation due to orbital precession insolation forcing of the African summer monsoon [11,13–16]. The interrelationship between the long-term and orbital-scale landscape changes is not well understood because long, continuous archives that capture both signals are rare, despite great efforts to find them [2,5,9,11,17–19]. Feakins *et al.* [11] presented plant wax $\delta^{13}C$ data from DSDP Site 231 in the Gulf of Aden and documented that the orbital-scale vegetation cycles were as large or larger than the long-term secular trend.

Our experimental design uses stable H- and C-isotopic analyses of terrestrial plant leaf wax biomarkers preserved in eastern Mediterranean Ocean Drilling Program (ODP) Site 967 for two 100 kyr-duration intervals centred near 3.05 and 1.75 Ma that bracket the East African C_4 vegetation increase. These windows were selected for their nearly identical orbital eccentricity ranges so that the orbital forcing would be comparable for each interval (figure 1). The goal of this study is to examine the relationship between short-term orbital and long-term secular changes in northeast African climate and vegetation across this Early Pleistocene (3–2 Ma) transition toward more open C_4 grasslands landscapes. Additionally, several samples were analysed for lignin monomer distributions to constrain the vegetation source of the leaf waxes. We further track orbital-scale Mediterranean surface conditions and sedimentological changes in response to African run-off variability through planktonic foraminiferal $\delta^{18}O$ and leaf wax concentration measurements. This study examines whether the East African vegetation transition between 3 and 2 Ma was accompanied by measureable changes in regional vegetation and climate responses to insolation forcing. This study only compares two short 100 kyr windows centred near 3.05 and 1.75 Ma, and thus it cannot address the larger, more encompassing question of whether there were

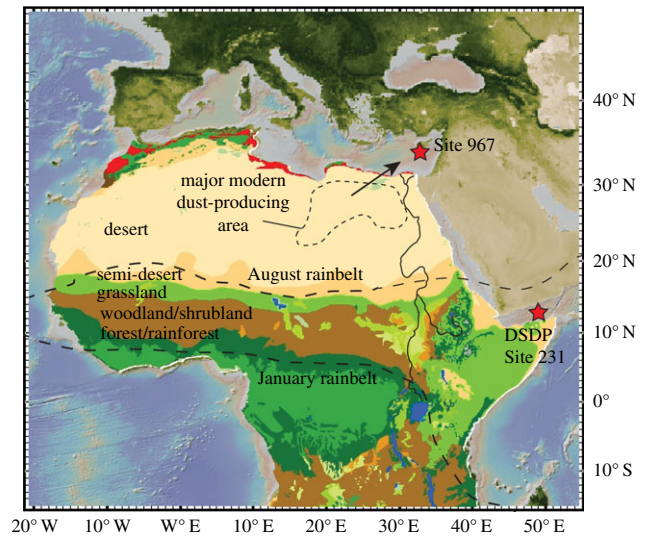


Figure 2. Modern vegetation and precipitation patterns in modern Africa. Vegetation transitions from tropical rainforest at the Equator to bare desert in the north [23]. The monsoonal rainbelt is approximately located in the Sahel during boreal summer and moves southward during austral summer [24]. ODP Site 967 is located in the eastern Mediterranean (red star) in the path of the Nile River outflow. The eastern Sahara (Algeria) is a major source of aeolian dust to the eastern Mediterranean today [25,26].

changes in African climate and vegetation responses to orbital insolation forcing throughout the Pliocene–Pleistocene.

2. Background

(a) Orbital and secular changes in North African climate and vegetation

The large meridional gradient from the humid Equator to the hyperarid Sahara desert in the northern African subtropics is expressed by a distinct zonation of climate and vegetation (figure 2). In northern subtropical Africa, strong monsoonal

circulation prevails, bringing precipitation during the Northern Hemisphere (NH) summer and a pronounced dry season during NH winter. A narrow fringe along the Mediterranean coastline receives wintertime precipitation and follows a typically Mediterranean climate [24]. Equatorial East Africa experiences a bimodal distribution of annual precipitation falling from March–May and October–November as the equatorial rainbelt passes over the Equator twice each year. North African vegetation tracks the precipitation gradient, as evidenced by the strongly zonal character of the rainforest, bushland, grassland and desert vegetation bands (figure 2).

Orbital precession regulates the seasonal distribution of solar radiation at the top of the atmosphere, but does not impact mean annual radiation receipt at a given latitude. During precessional index minima ($I = e^* \sin(\omega)$, where e is eccentricity and ω is the longitude of perihelion), summer season insolation is enhanced over northern subtropical Africa and this invigorates summer monsoonal circulation and its northward penetration into the subcontinent [27]. North African palaeoclimate records from palaeolake and marine sediments show that the Early Holocene African Humid Period (11–5 ka BP) was characterized by greater rainfall, reduced dust fluxes, larger lakes, increased grassland cover, reactivated ‘fossil’ river systems, groundwater recharge and high Nile River run-off into the Mediterranean Sea (e.g. [5,28–31]).

The eastern Mediterranean sedimentary record of sapropel deposition documents orbital precession forcing of North African climate since at least 10 Ma [14,21,32,33]. Sapropels are dark, organic-rich sediments (5–10% total organic carbon) that were deposited as a result of bottom-water anoxia due to surface water stratification from enhanced Nile River run-off and greater Mediterranean surface productivity [32–35]. North African run-off during sapropel periods was delivered to the eastern Mediterranean not only by the existing Nile River basin and its large Ethiopian highlands catchment, but also from ‘fossil’ river systems in Libya and Tunisia [36–39]. During North African dry periods, eastern Mediterranean sediments are dominated by carbonate-rich foraminiferal and nannofossil oozes with abundant aeolian dust [40]. A simple proxy for African run-off intensity such as sediment colour (lightness, L^*) captures the stark colour contrast between dark sapropel layers and light carbonate sediments [40]. Such records show prominent, precessionally paced bedding cycles that also exhibit characteristic longer-term orbital eccentricity modulation at 100, 400 and 1.2 Myr timescales [33]. Although impressive, the sapropel bedding cycles are not quantitative records of North African run-off because they record only a binary presence/absence of deep ocean anoxia related to variable African river run-off [40]. Aeolian dust supply to the eastern Mediterranean is principally derived from central Algeria and occurs during boreal spring [25,26]. Geochemical analyses of terrigenous sediments at ODP Site 967 document a well-defined aeolian end member composition consistent with this source area [41,42].

Precession-related changes in East African climate and vegetation are also well documented in East African palaeolake and offshore marine sediments. Lake Turkana in northern Kenya was 80 m higher than today during the Early Holocene Humid Period [13], and exhibited precessionally paced lake-level variability between 2.0 and 1.85 Ma [43], with evidence for high lake-level stands during eccentricity maxima [19]. Other East African lake basins such as Lake Challa [44], Lake Tanganyika [45] and the Horn of Africa region [45] were also

more humid at this time. Plant wax biomarker data from palaeolake Olduvai (Tanzania; 1.9–1.8 Ma) record large precessional variations in regional palaeohydrology and vegetation, with local landscapes cycling between closed C_3 woodlands and open C_4 grasslands [15,16].

Secular, long-term changes in East African climate and vegetation towards more arid and open conditions after ca 3 Ma have been documented in numerous studies based on both terrestrial and marine sediment sequences (figure 1; [2,9–12,18,46–48]). East African leaf wax biomarker and soil carbonate records (figure 1*c,d*) document a significant shift towards arid-adapted C_4 grasslands near 3 Ma, coincident with peaks in African mammal species richness and major steps in human evolution [8]. Dust flux, soil carbonate, pollen and fossil records document shifts towards open and more arid conditions during this same period near major global climate events, particularly between 3 and 2 Ma [1,7,10,12,18, 48–50] (figure 1). Although regional diversity in the timing and spatial patterns of open environments and C_4 expansion is apparent [2], East Africa experienced a broad, long-term trend towards more open landscapes between 4 and 1 Ma [2,9,18,48]. Orbital resolution sampling is not possible for many terrestrial records due to lithostratigraphic changes, limited age control and erosion/non-deposition, so it is challenging to evaluate the relationship between orbital and long-term climate variability for these sequences. For one deep-sea sediment record from the Gulf of Aden, the orbital-scale palaeovegetation amplitude was found to be comparable with the observed overall Pliocene–Pleistocene grassland expansion trend [11].

(b) ODP Site 967 and Mediterranean paleoclimate records

ODP Site 967 is located in the eastern Mediterranean basin on the northern slope of the Eratosthenes Seamount (34° N, 34° E, 2252 m) [51]. Long records of planktonic foraminiferal $\delta^{18}\text{O}$, African dust and Mediterranean sea surface temperatures (SSTs) exist for Site 967, allowing the proxy records developed in this paper to be compared with long-term northern African and Mediterranean trends [5,22,52]. Low-resolution alkenone SST estimates for Site 967 show that SSTs were fairly uniform at approximately 23°C before 2.2 Ma, varied between 18 and 20°C from 1.3 to 0.95 Ma, and between 14 and 22°C since 0.5 Ma [53]. An existing 3.2 Myr $\delta^{18}\text{O}_{\text{ruber}}$ record from Site 967 exhibits an orbital-pacing history similar to global $\delta^{18}\text{O}$ records [22]. Strong precessional and obliquity pacing dominates the $\delta^{18}\text{O}_{\text{ruber}}$ signal between 3 and 2 Ma, dominant obliquity pacing between 2 and 1 Ma, and strong eccentricity pacing from 1 to 0 Ma. Shifts in $\delta^{18}\text{O}_{\text{ruber}}$ variability at 2.6 and approximately 0.9 Ma are obvious, indicating that $\delta^{18}\text{O}$ in the Mediterranean recorded high-latitude climate shifts. Mediterranean seawater $\delta^{18}\text{O}$ ($\delta^{18}\text{O}_{\text{sw}}$) exhibits very large-amplitude orbital-scale variability (approx. 5‰) compared with open ocean $\delta^{18}\text{O}_{\text{sw}}$, due to the additional (large) influences of regional temperature, salinity and ice volume changes in the restricted basin [22]. Changes in precipitation–evaporation and river run-off led to salinity decreases of 1–8 practical salinity units (p.s.u.) during sapropel deposition [53,54]. Corresponding changes in $\delta^{18}\text{O}$ of seawater in response to salinity variability are approximately 0.4‰/1 p.s.u. [53,55]. Larrasoña *et al.* [5] constructed a continuous, 3 Myr dust record from Site 967 by measuring haematite concentration variability as a proxy for Saharan dust. Average dust concentrations were found to be

similar between 3 and 1 Ma, with large orbital-scale variability throughout.

(c) Terrestrial vegetation and climate proxies

The carbon isotope composition of sedimentary leaf wax 'biomarker' compounds provides a rigorous means by which to determine the photosynthetic pathway of the plants that produced them [56]. Plants use three major photosynthetic pathways today: C_3 (Calvin–Benson), C_4 (Hatch–Slack) and Crassulacean acid metabolism (CAM) [57]. The C_3 and C_4 notation refers to the number of carbon atoms in the first photosynthetic compound. Most trees, shrubs and herbs use the evolutionarily ancient C_3 pathway, characterized by relatively inefficient carbon and water utilization. Most tropical grasses and sedges use the C_4 pathway that evolved in response to reduced CO_2 conditions after the Late Oligocene. C_4 plants are distinguished by unique anatomical and biochemical adaptations that result in much more efficient carbon fixation and water utilization. Consequently, even though C_4 plants only represent about 3% of all land plant species, C_4 grasses and sedges represent 80% of terrestrial primary productivity across the warm tropics and subtropics as they are better adapted to seasonal heat and water stress [58].

In this study, we use leaf wax molecules preserved in eastern Mediterranean sediments to infer the mixture of C_3 versus C_4 plants growing on the landscape and the hydrogen isotopic composition of North African rainfall. Leaf waxes are composed of a large variety of very long, straight-chain (n) hydrocarbon compounds, including alkanes, carboxylic fatty acids and alcohols, which act as a protective coating on the leaf surface and help maintain water balance within the plant [59]. Leaf wax biomarkers can be transported to lake and marine sediments through fluvial transport, for example, with plant matter in a stream or river, or via aeolian transport [60–62]. The biomarkers and their isotope composition (hydrogen and carbon) are stable over many millions of years [63]. Studies of aerosol leaf wax $\delta^{13}C$ off the western margin of Africa have concluded that living plant leaf waxes dominated over 'old' leaf waxes associated with soil organic matter entrained by the wind [56,61].

Recent calibration work in North America, Europe and tropical Africa has supported the use of hydrogen stable isotopes from sedimentary leaf wax biomarkers to reconstruct rainfall δD values [60,64–67]. In the tropics and subtropics, δD_p is significantly influenced by the 'amount effect' in addition to temperature effects on Rayleigh fractionation [68]. The amount effect results in very depleted δD_p and $\delta^{18}O_p$ values during the rainy season in tropical Africa [69]. There is high positive linear correlation ($r^2 > 0.92$, $p < 0.001$) between the δD of precipitation (δD_p) and the δD of leaf waxes in the tropics and mid-latitudes, making δD_{wax} a good proxy for δD_p in a large variety of environments [67].

An additional proxy for terrestrial vegetation type is sedimentary lignin composition [70]. Lignins are phenolic polymers produced by vascular plants, which are dominantly terrestrial organisms [70]. In order to analyse lignin compounds, the polymers must be oxidized into individual monomers, which include aldehydes, acids and ketones [71]. Conventionally reported compounds are syringyl (S), cinnamyl (C) and vanillyl (V) yields. Gymnosperm and angiosperm vascular plants have different characteristic S/V and C/V ratios from each other and between their woody and non-woody tissues,

making lignins a useful proxy for vegetation source and the presence of terrestrial vegetation in sediments [70,72]. Grasses in particular have very high C/V ratios of greater than unity.

3. Methods

(a) Sampling and age model

We selected eastern Mediterranean ODP Site 967 for this study as it contains a nearly continuous, high-accumulation rate sediment record since the Pliocene, including all known sapropel cycles back to 3.2 Ma [40]. Site 967 is located on the flank of the Eratosthenes Seamount in the eastern Mediterranean and is dominated by African sediment deposition that derives from East Africa via the Nile River as well as from Saharan dust (figure 2; [21,73]). Sedimentation rates at Site 967 have averaged 2.6 cm per kyr since the Early Pliocene [40]. Aeolian dust supply to the eastern Mediterranean is derived principally from eastern Saharan dust sources in Algeria [25,26].

We sampled two 100 kyr-duration intervals centred near *ca* 1.75 and 3.05 Ma. These time periods were selected because they bracket the large increase in East African C_4 vegetation between 3 and 2 Ma (figure 1), and because these specific intervals have similar eccentricity amplitudes and calculated orbital precession forcing (figure 1, grey bars). This sampling allows us to quantify and compare regional hydroclimate and vegetation responses to orbital forcing for these specific time windows. Because the sampling is limited to these windows only, we cannot speak to the larger question of long-term, secular changes in orbital climate variability. ODP Site 967 sediments are composed of nanofossil clays, nanofossil oozes and organic matter-rich sapropels [40]. We sampled ODP Site 967 cores at 5 cm (2.5 kyr) spacing between 51.88 and 53.82 revised metres composite depth (RMCD) and 88.87–91.09 RMCD, or 1.68–1.78 Ma and 3.0–3.1 Ma in age, respectively. The age model of Emeis *et al.* [51] was employed to calculate sample ages via linear interpolation from sample depths on the RMCD scale [40].

To reconstruct regional hydroclimate variability we measured compound-specific hydrogen isotopic ratios from sedimentary leaf waxes (δD_{wax}). We construct a proxy record of regional vegetation variability by measuring compound-specific carbon isotope ratios in leaf waxes ($\delta^{13}C_{wax}$), and lignin was measured in selected samples to help clarify leaf wax provenance. We also have a qualitative proxy record of monsoonal river run-off to the eastern Mediterranean using $\delta^{18}O$ from planktonic foraminifera species *Globigerinoides ruber* (white).

(b) Plant wax biomarker analyses

Ground and homogenized samples were extracted using a Dionex accelerated solvent extractor (ASE) 350 with dichloromethane: methanol (DCM:MeOH) 9:1 at a temperature of 100°C and pressure of 1500 psi (10.34 MPa). Extraction of sufficient leaf wax compounds for gas chromatography (GC) analysis required 15–20 g of nanofossil ooze/clay sediments (hereafter referred to as nanofossil ooze) and approximately 5 g of sapropel sediments. Sediments were mixed with clean Ottawa sand in order to increase sediment permeability during ASE extraction, as nanofossil oozes in particular contain high amounts of clays. Total lipid extracts (TLEs) were spiked with a fatty acid internal standard (*cis*-11-eicosenoic acid) and dried at 30°C under nitrogen gas (N_2).

The TLEs were loaded onto a solid-phase aminopropyl (LC-NH₂) column in 2:1 dichloromethane:isopropanol (2:1 DCM:iso) and separated into neutral, acid and polar fractions (eluted with 4 ml 2:1 DCM:iso; 4 ml 4% acetic acid in ether (v/v); 4 ml methanol, respectively). Separated fractions were blown down to dryness under N_2 gas. The acid fractions were methylated by dissolving the fraction in 0.2 ml of DCM, adding

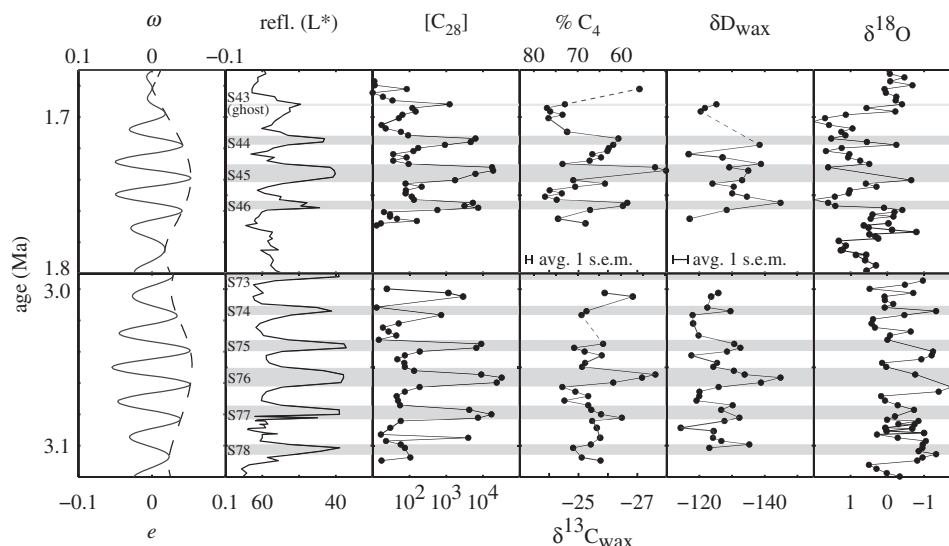


Figure 3. Results: no change in E. Saharan precipitation or vegetation from 3 to 1.67 Ma. Precession and eccentricity pacing are obvious across all proxy records in both time periods [20]. Sediment reflectivity (L^*) is a proxy for changes in sedimentology and carbon content and shows strong orbital pacing [40]. Sapropel locations are marked by grey boxes [22,51]. Concentrations of C_{28} FAMES (ng g^{-1} sediment) also closely follow orbital forcing (this study). $\delta^{13}\text{C}_{\text{wax}}$ (‰ versus VPDB, C_{28}) and $\delta\text{D}_{\text{wax}}$ (‰ versus VSMOW, C_{28}), corrected for $\delta^{13}\text{C}_{\text{CO}_2}$ changes and ice volume changes, respectively, exhibit strong precession pacing and similar average values from the older to the younger period (this study), indicating no change in vegetation composition or precipitation between the two times. $\delta^{18}\text{O}_{\text{ruber}}$ (corrected for ice volume changes (‰ versus VSMOW) measurements show strong precession pacing in the older period but lower frequency variability in the younger time period, indicating increased high-latitude climate influence on Mediterranean surface conditions in the Pleistocene.

1 ml acidified methanol (95:5 v/v mixture of methanol:acetyl chloride) and heating at 60°C overnight. Deionized water (1 ml) was added to the cool methylation mix and the methylated acids were extracted with hexane to isolate the methyl esters (approx. 1.5 ml hexane, repeated three times). Phthalic acid standards were methylated in parallel for determination and mass-balance correction of $\delta^{13}\text{C}$ and δD from the added methyl group. Fatty acid methyl esters (FAMES) were separated from other functionalized FAMES on silica gel columns (Aldrich, 70–230 mesh, 60A; DCM, methanol extracted, activated 2 h at 200°C). Samples were loaded in hexane onto the silica gel columns, and three fractions were collected (eluted with 4 ml hexane, 4 ml DCM, 4 ml methanol). The DCM fractions containing the methyl esters were dried gently under N_2 gas and transferred in hexane to 2 ml glass vials for GC analysis.

To track lithologic and organic carbon variability, we utilized the existing hole-specific colour reflectance (L^*) record of Site 967 and measured concentrations of long chain FAMES (figure 3) [40]. Reflectance was calculated for each sample depth via linear interpolation of the published data for each hole (ODP Site 967B and 967C) as appropriate. FAMES were analysed on a gas chromatography–flame ionization detector (GC-FID) for determination of compound abundances using the internal standard. Concentrations of $n\text{-C}_{28:0}$ FAMES (C_{28}) are reported in figure 3, with average replicate nannofossil ooze sample standard deviation (s.d.) of 0.35 (ng g^{-1} sediment) and replicate sapropel sample s.d. of 11.17 (ng g^{-1} sed.).

Compound-specific isotope values were analysed on a Thermo Trace GC Ultra coupled to a Thermo Delta V Plus isotope ratio mass spectrometer (GC-irMS) in duplicate to obtain δD and $\delta^{13}\text{C}$ values. The GC oven temperature was held at 60°C for 1.5 min, ramped at $30^\circ\text{C min}^{-1}$ to 225°C , then ramped at $10^\circ\text{C min}^{-1}$ to 325°C and held for 13 min. Internal laboratory standards (mixture of four FAME peaks of known concentration and unknown isotopic composition) and a standard mix of eight alkyl esters of known isotopic composition ('F8' FAME mix, obtained from Arndt Schimmelmann) were run alongside samples to calibrate isotope values to the Vienna Standard Mean Ocean Water (VSMOW) and Vienna pee dee belemnite (VPDB) scale. Pooled analytical uncertainties

(1 s.e.m.) were calculated after Polissar & D'Andrea [74]: $\delta\text{D}_{\text{wax}}$ and $\delta^{13}\text{C}_{\text{wax}}$ uncertainties were 4.8‰ and 0.25‰ , respectively [74]. Isotope values were adjusted for the methyl group addition through mass-balance corrections based on measurements of phthalic acid methyl esters; δD and $\delta^{13}\text{C}$ estimates of methanol stable isotope composition were $-180 \pm 7.5\text{‰}$ (non-exchangeable H) and $-25.5 \pm 0.9\text{‰}$, respectively. Uncertainty in these values is included in the uncertainty estimates above.

Hydrogen isotope measurements are automatically corrected by the operating software for isobaric contributions from H_3^+ produced in the ion source of the mass spectrometer, monitored daily. The H_3^+ factor was measured daily during analysis.

Nonlinear effects of isotope values over a range of CO_2 gas concentrations were observed in $\delta^{13}\text{C}_{\text{wax}}$ analyses in both sample and standard injections. A large range in sample C_{28} FAME concentrations (figure 3) made it difficult to inject compounds at higher concentrations to counteract this effect. Nonlinear behaviour in $\delta^{13}\text{C}$ measurements was corrected using repeat measurements of a sample along a large peak area range. While important, uncertainty in these corrections is not large enough to impact the findings of this study.

Changes in ice volume over time affect the isotopic composition of rainfall, which in turn is recorded by $\delta\text{D}_{\text{wax}}$ and $\delta^{18}\text{O}_{\text{ruber}}$ [60,75]. We correct for these changes by using the benthic $\delta^{18}\text{O}$ stack of Lisiecki [76], which records changes in ice volume and deep-sea surface temperatures. We adjust the $\delta^{18}\text{O}_{\text{stack}}$ such that the youngest value is equivalent to modern seawater $\delta^{18}\text{O}$ values. We then divide the adjusted values by the last glacial maximum $\delta^{18}\text{O}_{\text{stack}}$ value (1‰) to scale the stack to the ice volume component of $\delta^{18}\text{O}_{\text{seawater}}$ [77]. Next, we calculate expected δD changes from ice volume ($\delta\text{D}_{\text{IV}}$), using the observed 8:1 relationship of δD versus $\delta^{18}\text{O}$ in modern precipitation [68,78]. The expected $\delta\text{D}_{\text{IV}}$ (δ_{accepted}) was interpolated at sample ages, and ice volume-corrected sample $\delta\text{D}_{\text{wax}}$ values ($\delta\text{D}_{\text{IVC}}$) were calculated. The effect of this correction on $\delta\text{D}_{\text{wax}}$ is shown in figure 4.

The photosynthetic pathway of the plant, water use efficiency and ambient atmospheric CO_2 $\delta^{13}\text{C}$ all combine to influence $\delta^{13}\text{C}_{\text{wax}}$ values [80]. We corrected $\delta^{13}\text{C}_{\text{wax}}$ values for changing $\delta^{13}\text{C}_{\text{CO}_2}$ since 3.12 Ma to pre-industrial $\delta^{13}\text{C}_{\text{CO}_2}$ values (-6.5‰)

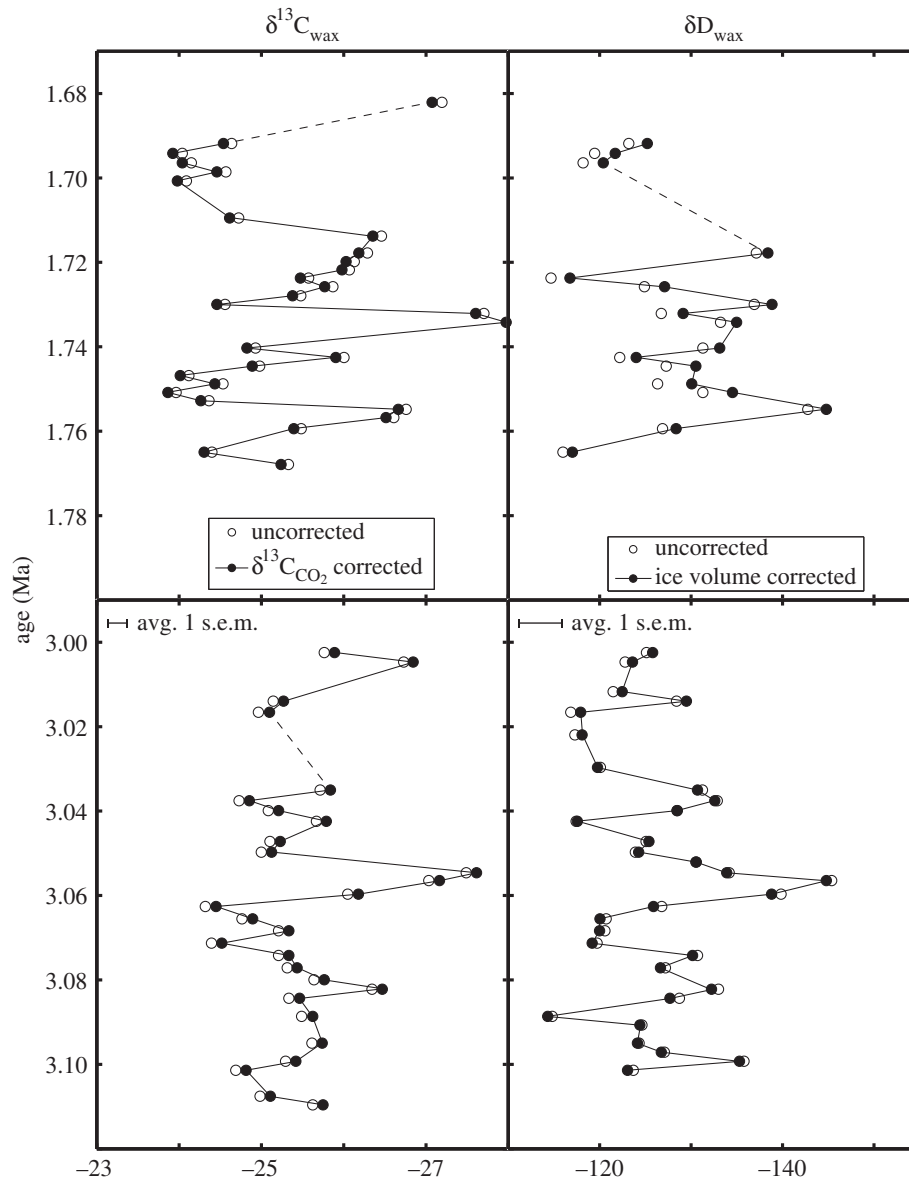


Figure 4. Effects of corrections on Site 967 isotope values. $\delta^{13}\text{C}_{\text{wax}}$ is corrected for changes in atmospheric $\delta^{13}\text{C}_{\text{CO}_2}$ (3 Myr running average) over time [79]. $\delta\text{D}_{\text{wax}}$ is corrected for changes in $\delta\text{D}_{\text{precipitation}}$ due to ice volume variability over time [76]. See §3 for details of these corrections.

Table 1. Published vegetation end member $\delta^{13}\text{C}_{\text{wax}}$ data.

veg. type	year collected	$\delta^{13}\text{C}$ atm. CO_2 (mean annual; versus VPDB) ^a	measured compound	$n\text{-C}_{28}^b$ $\delta^{13}\text{C}_{\text{CO}_2,\text{corr.}}$	source
C ₄ grass	1997, 1998, 2000	−7.952, −8.048, −8.052	n-acid C ₂₈	−20.5	Chikaraishi <i>et al.</i> [82,83]
C ₄ grass	1989	−7.8	n-alkane C ₂₇	−21.3	Collister <i>et al.</i> [84]
C ₃ angiosperm trees	1999, 2000	−8.035, −8.052	n-acid C ₂₈	−35.4	Chikaraishi <i>et al.</i> [82,83]
C ₃ savannah trees	1992, 2003, 2005	−7.838, −8.161, −8.216	n-alkane C ₂₇	−31.7	Vogts <i>et al.</i> [85]

^a $\delta^{13}\text{C}_{\text{CO}_2}$ data are from Francey *et al.* [86] (pre-1978) and Keeling *et al.* [87] (1980–2008). $\delta^{13}\text{C}_{\text{wax}}$ measurements were corrected to the 1861 $\delta^{13}\text{C}_{\text{CO}_2}$ value of −6.49‰, using the ϵ equation.

^bAverage ϵ $n\text{C}_{27} - n\text{C}_{28}$ is 0.9‰ for C₃ plants, and 1.0‰ for C₄ plants [83].

using the $\delta^{13}\text{C}_{\text{CO}_2}$ of Tipple [79]. The effect of this correction on $\delta^{13}\text{C}_{\text{wax}}$ is shown in figure 4.

We examine sedimentary leaf wax provenance using lignin compounds for two samples spanning the largest $\delta^{13}\text{C}_{\text{wax}}$ range observed in our records. One sapropel and one nannofossil ooze sample, dating to 1.73 and 1.75 Ma, respectively, were analysed for lignin monomers at the Stable Isotope Biogeochemistry

Laboratory, Purdue University. Samples were prepared after [81].

To calculate the percentage of C₄ vegetation present in each sample, a variety of C₄ and C₃ $\delta^{13}\text{C}$ end members were collected from the literature, corrected to pre-industrial $\delta^{13}\text{C}$ and used in a variety of linear mixing lines to calculate a range of possible C₄ percentages (table 1). Chikaraishi *et al.* [82]'s fatty acid values for C₄

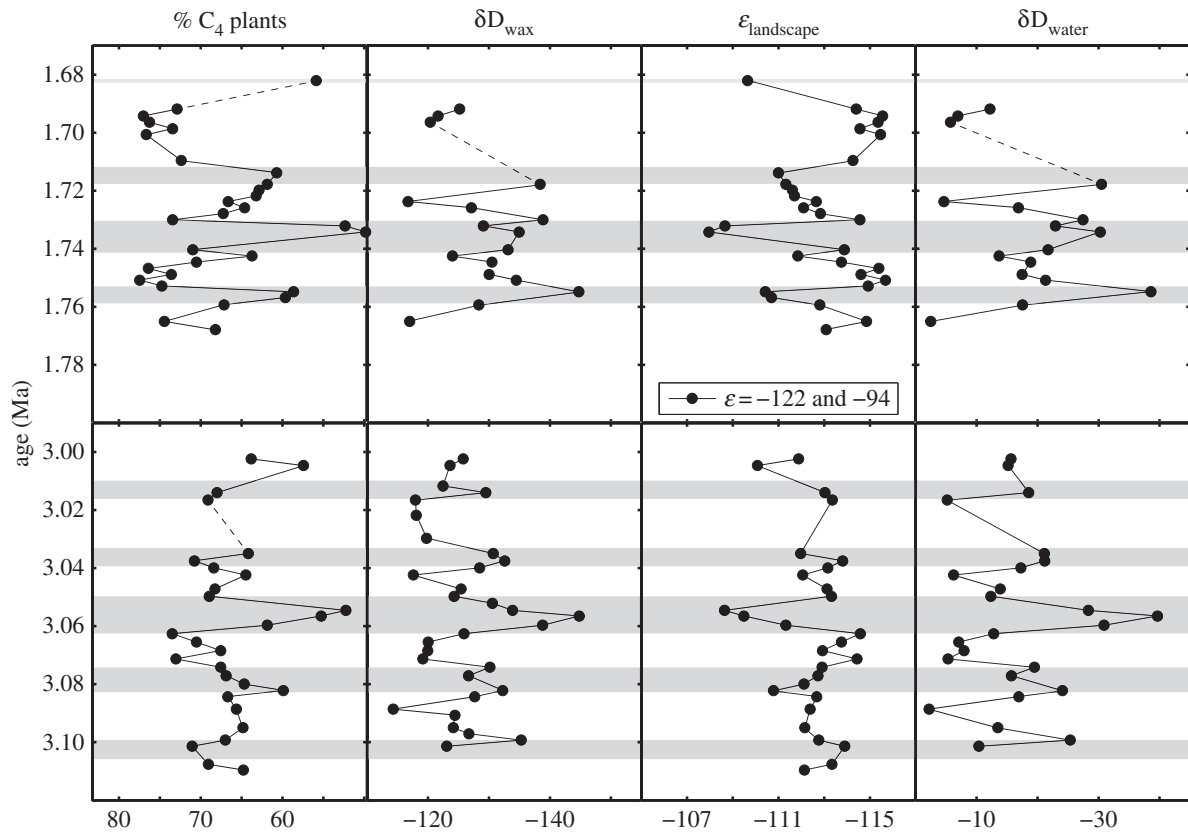


Figure 5. Potential impacts of vegetation change on plant source water δD (δD_{water}) calculations. C_4 vegetation calculations are shown in the first column (calculated via linear interpolation with C_3 and C_4 vegetation end members of -35.4% and -20.5% , respectively; [83]). The second column shows ice volume-corrected δD_{wax} ($\%$ versus VSMOW). The third column displays $\epsilon_{\text{landscape}}$ calculations from a two-end-member linear mixing model; end member values are indicated in the top (figure 3) [83]. The last column shows δD_{water} ($\%$ versus VSMOW) calculations made by correcting δD_{wax} . δD_{water} variability is slightly larger amplitude than that of δD_{wax} . Averages of δD_{water} are not significantly different from the older to the younger interval.

grass and C_3 angiosperm trees were chosen as the final end members in our analysis [82] (figure 3). We attempted to account for potential effects of vegetation change on δD_{wax} values using $\delta^{13}\text{C}_{\text{wax}}$ measurements and modern apparent fractionation factors (epsilon factors, ϵ) (table 1). We selected average ϵ values (for C_{28} n-acids) of -94% and -122% , respectively, for C_3 angiosperm trees and C_4 grasses measured in modern plants [64], calculated an ' $\epsilon_{\text{landscape}}$ ' (after Magill *et al.* [88]) for each δD_{wax} measurement using C_4 grass percentage calculations (described above), and applied the $\epsilon_{\text{landscape}}$ to each δD_{wax} value to reconstruct δD_{water} [16,82] (figure 5).

(c) Planktonic foraminifera analyses

The planktonic foraminifera *G. ruber* (white; 250–300 μm) was used as a proxy for surface ocean conditions, particularly temperature and salinity. Five to seven whole foraminifera were picked from each sample (250–355 μm fraction), and cleaned with repeated MilliQ water rinses to remove clay and organic matter prior to transfer into acid-cleaned vials for analysis. Nannofossil ooze sediments contained abundant *G. ruber*, but some sapropel sediments were devoid of planktonic foraminifera or did not contain enough *G. ruber* for analysis. Samples were analysed at LDEO for $\delta^{18}\text{O}$ and $\delta^{13}\text{C}$ ($\delta^{18}\text{O}_{\text{ruber}}$ and $\delta^{13}\text{C}_{\text{ruber}}$) on an Isoprime 100 multicarb dual-inlet isotope mass spectrometer; approximately 10% of samples were run in duplicate to assess sample standard deviation (s.d.). International carbonate standard NBS-19 was analysed alongside samples. Long-term s.d. for $\delta^{18}\text{O}$ and $\delta^{13}\text{C}$ were 0.06 $\%$ and 0.04 $\%$, respectively, based on repeat analyses of NBS-19. Standard deviation of replicate samples was 0.20 $\%$ and reflects both analytical uncertainty and sampling variability of the distribution of *G. ruber* individuals in a sample.

4. Results

(a) Orbital-scale variability

Precession-scale (approx. 20 kyr) variability is predominant in all measured proxies (figure 3). Figure 3 shows eccentricity-modulated precession calculations, which are very similar for the two periods [20]. Reflectivity of sediments mirrors precession variability with a slight lag (3 kyr, built in from the age model), with more reflective nannofossil ooze sediments deposited near precession maxima and less reflective, sapropelic sediments deposited near precession minima (figure 3). Reflectance amplitudes are similar to eccentricity-modulated precession amplitudes in the younger period, but are less similar in the older period, i.e. reflectance unit minima are relatively constant around 40 (L^*).

Concentrations of C_{28} n-acids vary over four orders of magnitude between high reflectivity sediments and sapropelic sediments, with highest concentrations (greater than 10^3 ng g^{-1} sediment) deposited during sapropel intervals (figure 3). These observations are consistent with enhanced organic matter preservation during sapropel formation due to bottom-water anoxia in the Mediterranean Sea [89] and potentially higher local leaf wax production in the humid, vegetated Sahara region. Sedimentary geochemical analysis of these Site 967 sediments indicates significant contributions of Nile-derived sediments during sapropel deposition and this may also have provided another plant wax source vector [42,90], but the several orders of magnitude higher plant wax concentrations cannot be explained by this additional, fractional source.

Table 2. Computing Pearson's correlation coefficients and significance for correlation of δD_{wax} and $\delta^{13}\text{C}_{\text{wax}}$.

	<i>r</i> -values	<i>p</i> -values
1.75 Ma $\delta^{13}\text{C}_{\text{wax}}$ versus δD_{wax}	0.35	0.20
3.05 Ma $\delta^{13}\text{C}_{\text{wax}}$ versus δD_{wax}	0.48	0.02

Large negative excursions of 2–3‰ (approx. 15–20% C_4) and 15–20‰ occur in $\delta^{13}\text{C}_{\text{wax}}$ and δD_{wax} , respectively, around and during sapropel sediments in both periods (figure 3), which is consistent with observations of recent precession-forced changes in North African vegetation and rainfall [30,91]. More negative $\delta^{13}\text{C}_{\text{wax}}$ is indicative of less C_4 plant abundance during sapropel intervals [80]. Corrections for $\delta^{13}\text{C}_{\text{CO}_2}$ and ice volume resulted in insignificant adjustments to $\delta^{13}\text{C}_{\text{wax}}$ and δD_{wax} (figure 4). Using Pearson's correlation coefficient, we found that δD_{wax} shows fairly high, very significant positive correlation with $\delta^{13}\text{C}_{\text{wax}}$ in the older period and slightly lower positive correlation in the younger period, in line with the expected close correspondence between precession forcing and leaf wax stable isotope patterns (table 2). This is also consistent with evidence that sapropels are deposited in response to more humid, vegetated North African conditions and vice versa [5,73,92].

The δD_{wax} records exhibit variability consistent with precessional forcing of monsoonal rainfall changes [44,67,93]. The amplitude of the Site 967 δD_{wax} cycles is about 20–30‰, which is comparable with the δD_{wax} amplitude for the Early Holocene African Humid Period in the Gulf of Aden, and Lake Tanganyika and Lake Challa [29]. Our calculations of source water δD (δD_{water}) reveal slightly larger variability across precession cycles due to the effect of correcting for vegetation changes from $\delta^{13}\text{C}_{\text{wax}}$ (§3b), but δD_{water} is similarly dominated by precession-scale variability (figure 5).

Even though we have only two lignin analyses, these are useful in constraining potential plant wax vegetation source changes between a wet and dry interval. Lignin analyses show very similar S/V and C/V ratios in both the sapropel and nannofossil ooze samples and are consistent with a grass-dominated vegetation source in both time periods (figure 6 and table 3). The nannofossil ooze has a slightly lower S/V ratio than the sapropel, but a nearly identical C/V ratio, consistent with very similar vegetation source. No syringyl aldehyde was detectable in the nannofossil ooze sample; therefore, we can only discuss the vanillyl acid/aldehyde (Ad/Al)_v ratio here as a measure of lignin preservation. The sapropel sample exhibits much higher (Ad/Al)_v than the nannofossil ooze, suggesting that lignin compounds in that sample underwent greater oxidation prior to deposition [70].

Variability in $\delta^{18}\text{O}_{\text{ruber}}$ is similar though not identical to that of sediment reflectivity, C_{28} FAME concentrations, δD_{wax} and $\delta^{13}\text{C}_{\text{wax}}$ during both periods (figure 3). Negative excursions of approximately 1.5–2‰ occur near sapropel mid-points, consistent with evidence that sapropels are deposited contemporaneously with large decreases in Mediterranean surface salinity due to increased African run-off [22].

(b) Long-term, secular changes in lipid and foraminifera stable isotope values

A Mann–Whitney/Wilcoxon rank sum test revealed no significant differences in $\delta^{13}\text{C}_{\text{wax}}$ means between the 3.05 and

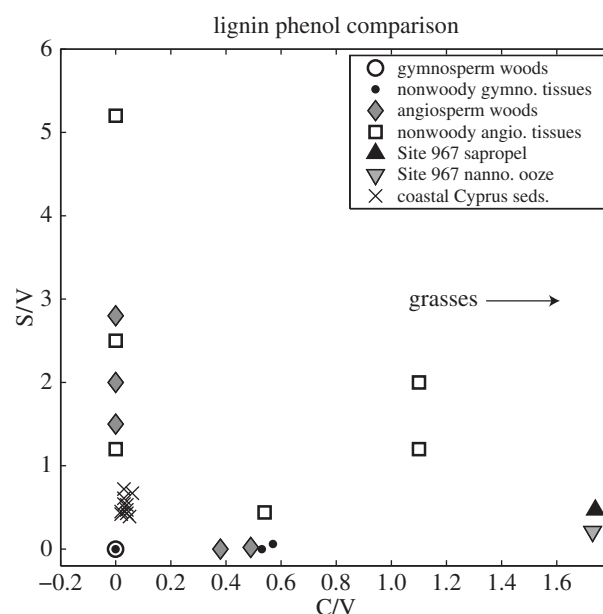


Figure 6. Site 967 lignin analyses support an eastern Saharan vegetation source. Site 967 lignin phenol data are compared above with published syringyl/vanillyl (S/V) versus cinnamyl/vanillyl (C/V) data from modern plants and a coastal Cyprus marine sediment core located just north of the Eratosthenes Seamount [70]. Grasses exhibit high C/V ratios relative to gymnosperm and angiosperm trees [70]. Site 967 samples exhibit high C/V ratios and relatively low S/V ratios, indicating a grass-dominated vegetation source consistent with eastern Saharan environments.

1.75 Ma windows. This result suggests that the vegetation and palaeohydrologic responses to orbital precession monsoonal forcing were comparable for these two time periods. The results cannot, of course, be used to infer conclusions about unsampled intervals, but they do suggest nearly identical means and variance for these time windows that bracket an important increase in C_4 vegetation in East Africa [2].

Curiously, the Site 967 $\delta^{13}\text{C}_{\text{wax}}$ results do not indicate a significant increase in C_4 vegetation for the 1.75 Ma interval compared with the 3.05 Ma interval, as was anticipated given the clear C_4 increases over this time period noted across many localities in East Africa [2,9] (figure 1). While it is possible our sampling strategy was not sufficient to capture this signal, our data for these two windows show high C_4 contributions (50–80% C_4) for both intervals, with no significant difference between them. This observation leads to the tentative conclusion that eastern Sahara vegetation evolution may have been separate from that observed in East Africa, a topic that we expand upon below.

The African run-off proxy, $\delta^{18}\text{O}_{\text{ruber}}$, does show highly significantly more positive values in the younger period after correcting for ice volume changes (table 4). Orbital-scale variability in $\delta^{18}\text{O}_{\text{ruber}}$ is also slightly larger in the 1.68–1.78 Ma period relative to the 3.0–3.1 Ma period. Regional and global temperatures have decreased since the Late Pliocene, making this a relevant factor for the Site 967 record (figure 7) [52,95].

5. Discussion

(a) Leaf wax provenance and interpretation of Site 967 $\delta^{13}\text{C}_{\text{wax}}$ and δD_{wax} results

Aeolian dust supply to the eastern Mediterranean is principally derived from central Algeria and occurs during boreal

Table 3. Lignin data from this study.

sample	sed. type	$\delta^{13}\text{C}_{\text{wax}}$	S/V	C/V	(Ad/Al) _V	(Ad/Al) _S
967B6H4, 147 cm	sapropel	−25.8	0.47	1.74	0.62	0.96
967B6H5, 32 cm	nanno. ooze	−21.5	0.21	1.73	0.32	—

Table 4. Average values and standard deviations for measured $\delta^{13}\text{C}_{\text{wax}}$, $\delta\text{D}_{\text{wax}}$ (ice volume-corrected) and $\delta^{18}\text{O}_{\text{ruber_ivc}}$ between 1.68–1.8 Ma and 3.0–3.1 Ma intervals.

	mean 1.75 Ma	mean 3.05 Ma	s.d. 1.75 Ma	s.d. 3.05 Ma
$\delta^{13}\text{C}_{\text{wax}}$	−25.32	−25.58	1.13	0.74
% C ₄	67.63	65.91	7.59	4.98
$\delta\text{D}_{\text{wax}}$	−133.8	−126.3	10.8	6.7
$\delta\text{D}_{\text{water}}$	−19.2	−16.2	10.6	8.9
$\delta^{18}\text{O}_{\text{ruber}}$	0.092	−0.432	0.668	0.577

spring [25,26]. Inorganic geochemical sediment provenance studies of haematite, ^{87}Sr isotope ratios, and major and minor elements of eastern Mediterranean sediments also suggest a dominantly northeastern Sahara source for dust transported into the eastern Mediterranean [5,73,96]. Wehausen & Brumsack [41], using major element ratios of sapropel sediments from eastern Mediterranean drill sites, found they were mainly (up to 100%) composed of inorganic sediments derived from the Nile River drainage basin, whereas drier (non-sapropel) periods were composed of 50% Nile River sediments and 50% Saharan dust.

A recent study of n-alkane and n-acid compounds in fluvial sediments in the Ganges and Brahmaputra River systems found that vascular plant material is a significant part of river organic carbon, and that these compounds reflect local vegetation composition in their respective drainage basins [97]. They observed a downstream enrichment of $\delta^{13}\text{C}_{\text{wax}}$ in both compound types that they interpreted as degradation and progressive replacement of fluvial sedimentary leaf wax compounds by mixed C₃/C₄ vegetation, particularly in the Ganges floodplain where C₄ vegetation dominates. This has important implications for Nile River fluvial leaf wax transport: as the Nile River is over twice as long as the Ganges and Brahmaputra Rivers, it might be expected that leaf wax compounds sourced from Nile headwaters would be completely replaced by downstream and floodplain leaf waxes before being deposited in the eastern Mediterranean Sea.

Based on these studies, we suggest that leaf waxes deposited in eastern Mediterranean sediments record a proximal vegetation source area in the eastern Sahara region, with some contribution from fluvially derived leaf waxes. Pollen reconstructions from the African Humid Period indicate that steppe vegetation (grasses, low shrubs) was abundant above approximately 20° N, and that savannah vegetation (annual grasses and scattered trees) was abundant between approximately 10–20° N, indicating an incursion of vegetation into presently bare desert regions [98,99]. This vegetation would have provided abundant additional leaf wax sources to rivers and streams draining into the eastern Mediterranean.

Modern spatial distributions of vegetation and pollen reconstructions of Mid-Holocene vegetation suggest that the Sahara/Sahel regions are dominated by C₄ vegetation during both wet and dry periods [100].

We conclude that C₄ grasses dominated northeast African environments in both the older and younger periods, with higher percentages of C₄ grasses during dry periods and lower percentages during humid periods, as indicated by $\delta^{13}\text{C}_{\text{wax}}$ and $\delta\text{D}_{\text{wax}}$ variability. On average, C₄ grasses comprise between 55 and 80% of total vegetation (figure 3), consistent with an eastern Saharan vegetation assemblage [98,101]. Our lignin results provide an additional test of sedimentary leaf wax provenance. High C/V ratios in both samples indicate a non-woody, grass-dominated lignin source [70]. This observation is consistent with high average C₄ grass abundance inferred from $\delta^{13}\text{C}_{\text{wax}}$ data (figure 4) and supports our conclusion that the eastern Sahara is the dominant source of terrestrial leaf waxes found in eastern Mediterranean sediments.

The observed minima in $\delta\text{D}_{\text{wax}}$, $\delta^{13}\text{C}_{\text{wax}}$ and $\delta^{18}\text{O}_{\text{ruber}}$ during sapropel periods are consistent with interpretation of these proxies as a means of tracking African monsoon strength and run-off. Sapropels have been observed to lag precession minima by approximately 3 kyr and correspond to peak monsoon run-off from Africa into the Mediterranean Sea [21,34]. Minima in $\delta\text{D}_{\text{wax}}$, $\delta^{13}\text{C}_{\text{wax}}$ and $\delta^{18}\text{O}_{\text{ruber}}$ appear to covary with the L* proxy for sediment colour reflectance and orbital insolation forcing (figure 3a), which supports our interpretations that $\delta\text{D}_{\text{wax}}$ tracks African monsoon rainfall to the eastern Sahara region, $\delta^{13}\text{C}_{\text{wax}}$ records vegetation changes responding to precipitation variability, and $\delta^{18}\text{O}_{\text{ruber}}$ captures Mediterranean Sea surface salinity and temperature changes in addition to ice volume. Precession-scale $\delta^{13}\text{C}_{\text{wax}}$ variability ranges approximately 2–4‰ (ca ±15–20% C₄ vegetation), much less than the 14‰ average difference between C₃ and C₄ vegetation, suggesting a mix of C₃ and C₄ vegetation across precessional cycles rather than oscillations between end members [102].

Depletion of $\delta\text{D}_{\text{wax}}$ and $\delta^{13}\text{C}_{\text{wax}}$ in response to precession-paced monsoonal precipitation maxima has been observed in numerous records throughout Africa, though some studies have found significant correlations between northern African climate variability and high-latitude climate and ocean circulation variability for the Late Pleistocene [16,45,62,103]. The range in orbital-scale $\delta\text{D}_{\text{wax}}$ and $\delta\text{D}_{\text{water}}$ amplitudes (approx. 20‰; figure 5) is reasonable when compared with Late Pleistocene $\delta\text{D}_{\text{wax}}$ data from tropical Africa. Tierney *et al.* [45] analysed $\delta\text{D}_{\text{wax}}$ records from the Congo Basin [93], Lake Tanganyika and Lake Challa between 0 and 25 ka, and observed approximately 20–30‰ shifts bracketing the African Humid Period. Collins *et al.* [103] observed orbital-scale $\delta\text{D}_{\text{wax}}$ variability of approximately 10–15‰ in Late Pleistocene northwest African margin marine sediments [103].

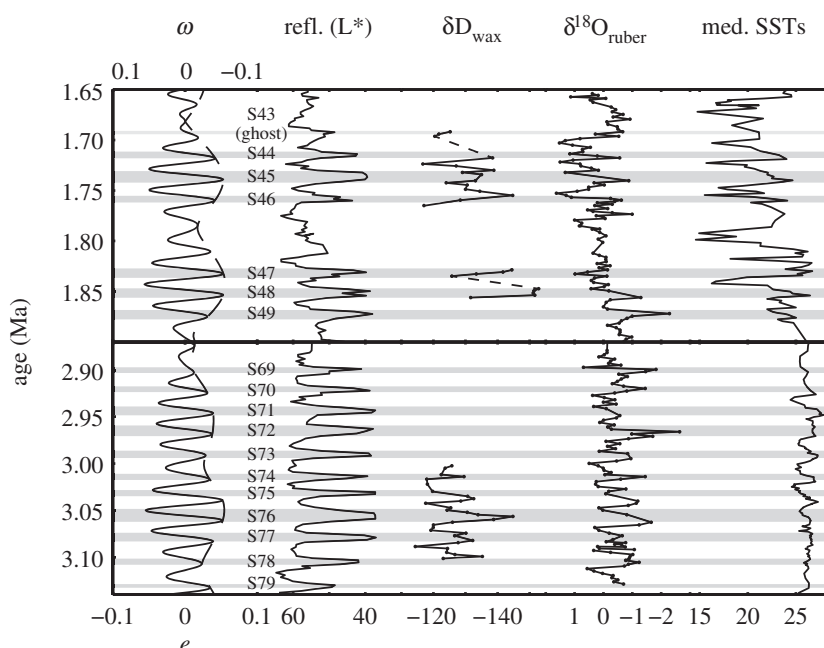


Figure 7. Mediterranean Sea surface conditions show increasing high-latitude influence from the Late Pliocene to Mid-Pleistocene. Shown above from left to right are orbital eccentricity (black dotted line) and precession (red line; [20]); sapropel numbers [94]; sediment reflectivity [40]; δD_{wax} (this study); $\delta^{18}O_{ruber}$ (this study) and Mediterranean SSTs [52]. Site 967 $\delta^{18}O_{ruber}$ exhibits two distinct patterns of behaviour in the Late Pliocene and Mid-Pleistocene. During the Late Pliocene period, $\delta^{18}O_{ruber}$ shows great resemblance to sediment reflectivity and δD_{wax} , varying primarily at approximately 20 kyr frequencies and suggesting that eastern Mediterranean $\delta^{18}O_{seawater}$ was controlled by salinity variability and African monsoonal run-off. During the Mid-Pleistocene, $\delta^{18}O_{ruber}$ shows longer periodicities and greatest resemblance to Mediterranean SSTs, strongly implying that SST was the primary control on $\delta^{18}O_{seawater}$ at this time, with sea surface salinity acting as a secondary control.

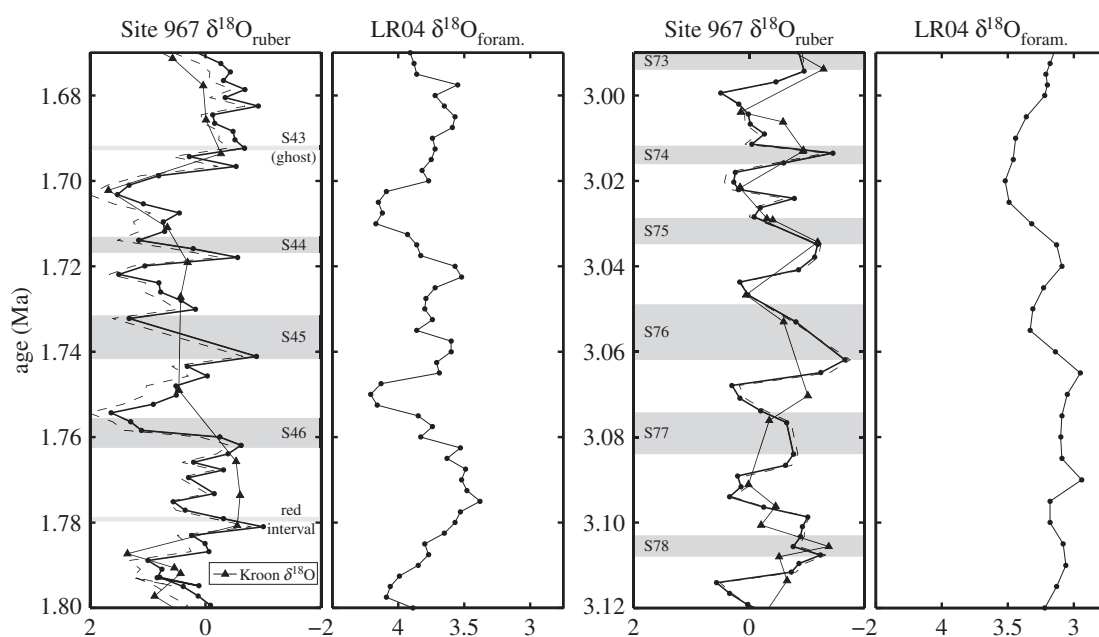


Figure 8. Site 967 $\delta^{18}O_{ruber}$ (this study) comparison with previously published Site 967 $\delta^{18}O_{ruber}$ and a global benthic foraminifera $\delta^{18}O$ stack [22,76]. Ssapropel intervals are shown by grey boxes and labelled 'S#'; a possible oxidized sapropel is denoted by a 'red interval' at 1.78 Ma [22,51]. High-resolution sampling at Site 967 (black dots) revealed approximately 20 kyr frequency variability not always captured by low-resolution sampling (black triangles). Site 967 $\delta^{18}O_{ruber}$ more greatly resembles global variability (LR04) from 1.67 to 1.8 Ma than between 3 and 3.12 Ma, suggesting that high-latitude climate has greater influence over Mediterranean surface conditions in the younger interval.

(b) Comparing Site 967 results with East African palaeoclimate and palaeovegetation records

The eastern Mediterranean Site 967 plant wax δD_{wax} and $\delta^{13}C_{wax}$ results document clear orbital-scale changes in regional hydrology and vegetation for the eastern Sahara

catchment region. The $\delta^{13}C_{wax}$ results suggest there was no significant difference in the mean value or variance between the 1.75 and 3.05 Ma intervals that were sampled. Moreover, we show that the values are consistent with an average 65% C_4 contribution for both periods, varying between 55 and 80% at the orbital-scale. The δD_{wax} results similarly

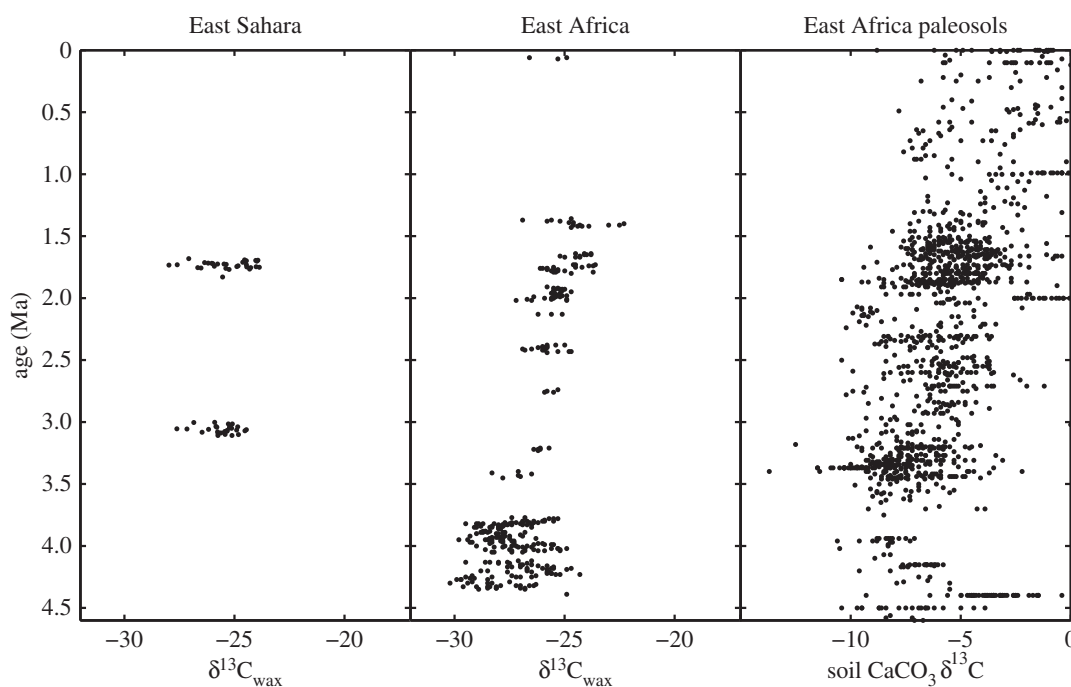


Figure 9. Site 967 (C_{28}) $\delta^{13}C_{wax}$ are compared with Gulf of Aden DSDP Site 231 (C_{30}) $\delta^{13}C_{wax}$ and East African soil carbonate $\delta^{13}C$ records [2,12]. Soil carbonate data markers (legend) are plotted from north to south and show vegetation data nearest to the Nile River headwaters in Ethiopia, also the primary source region for Nile sediments [105]. Average Site 967 $\delta^{13}C_{wax}$ remains constant between the approximately 3.05 Ma and approximately 1.75 Ma windows, while Site 231 $\delta^{13}C_{wax}$ and palaeosol $\delta^{13}C$ record a clear shift towards more positive values across the same interval, implying that East Saharan vegetation remained constant while East Africa transitioned towards more abundant C_4 grasslands.

document comparable mean values between the 1.75 and 3.05 Ma intervals, with comparable orbital-scale amplitudes (approx. 20–30‰) under comparable orbital eccentricity and precession forcing (table 4). These amplitudes are comparable to multiple plant wax δD_{wax} records of the Early Holocene African Humid Period [29].

Site 967 records some climate signals that are restricted to the eastern Mediterranean sector. The lower frequency variability (approx. 40 kyr) of $\delta^{18}O_{rubber}$ in the younger period is likely related to the influence of high-latitude climate on Mediterranean SSTs based on a comparison with a newly developed alkenone record of Mediterranean SST variability [52] (figure 7). Variations in $\delta^{18}O_{rubber}$ between 1.68 and 1.8 Ma show greater similarity to central Mediterranean Uk'37 SSTs than to sediment reflectivity, δD_{wax} and $\delta^{13}C_{wax}$. This supports the assertion that the Mediterranean region shows increasing high-latitude climate influence throughout the Pliocene and Pleistocene [22,52]. However, the similarity of $\delta^{18}O_{rubber}$ and central Mediterranean SSTs may suggest that SST variability (in excess of 5–8°C for the ca 1.75 Ma interval) increasingly influences Mediterranean $\delta^{18}O_{rubber}$ over the Pleistocene [22,52]. There is also great similarity between Site 967 $\delta^{18}O_{rubber}$ and the global $\delta^{18}O$ stack, further indicating that high-latitude climate change influenced Mediterranean surface conditions (figure 8). This implies that Mediterranean surface conditions did not dominantly influence precipitation or vegetation changes in the plant wax catchment area (eastern Sahara) for Site 967, and that precessional monsoonal climate forcing was the predominant climate signal here.

Our results can only speak to the short intervals that were sampled near 3.05 and 1.75 Ma, but they do suggest that there was little change in the monsoonal palaeohydrological or palaeovegetation response to monsoonal circulation changes for these two time intervals which bracket the onset of NH glaciation after 2.8 Ma [104] as well as the shift toward more open, C_4 -dominated landscapes in East Africa [2].

(c) Regional differences in northeast African vegetation change

We reach the conclusion that there was no change in eastern Saharan hydroclimate or vegetation response to orbital monsoonal forcing for these 3.05 and 1.75 Ma windows. Furthermore, the Site 967 $\delta^{13}C_{wax}$ means and standard deviations for these two windows are indistinguishable (table 4) suggesting (but not proving) that there was no secular change between these windows. This contrasts with the well-documented increase in C_4 vegetation at many, but not all, East African sites and offshore marine sediments [2,9,11,12]. To reiterate, additional sampling is required to confidently assert that the Site 967 results do not conform to the East African vegetation history, but our initial results support this view. Extracting all palaeosol $\delta^{13}C$ values for these same sampled time periods from the Levin & Naoami [2] database indicates there is a significant increase in mean values between the 1.68 and 1.8 Ma window ($-5.0 \pm 1.5\%$, $n = 101$) and the earlier 3.0–3.15 Ma window ($-7.6 \pm 1.8\%$, $n = 9$; figure 9).

Given the eastern Sahara dust source area provenance for Site 967 and the lack of a significant $\delta^{13}C_{wax}$ change between our older and younger intervals, we conclude that the eastern Sahara may have had a distinctly different vegetation history from East Africa, and that the well-known C_4 increase in East Africa was, in fact, restricted to this geographical domain. Our results would suggest that the eastern Sahara experienced large-amplitude C_3 – C_4 vegetation and palaeohydrological cycles with no evidence for a shift to more open or more varied conditions. By contrast, East African localities, collectively, indicate a marked expansion of C_4 vegetation towards more open landscapes between 3 and 2 Ma [2,9,11,48,106]. Moreover, where detailed, sub-orbital sampling has been performed for lacustrine intervals (palaeolake Olduvai), palaeovegetation inferences from plant wax $\delta^{13}C$

data indicate full amplitude 0–100% C_4 vegetation cycles tracking orbital precession near 1.9–1.8 Ma [15,16]. If supported by additional analysis, our results suggest that the 3–2 Ma expansion of C_4 vegetation and shift to more open East African landscapes may have been restricted to the East African domain and was not a pan-African vegetation transition. More analysis is required to support this assertion but available data support this view.

One mechanism has been proposed that could explain why East African vegetation shows such a well-defined shift to more open, C_4 -rich vegetation after 3–2 Ma. An emerging view proposes that East Africa became drier in response to changes in tropical ocean temperature gradients during the Early Pleistocene [107,108]. Where tropical SSTs are warmest, such as the IndoPacific warm pool, the overlying atmosphere saturates with water vapour and convects. The resulting rainfall and latent heat release drive a large-scale overturning cell, the Walker circulation. The compensatory dry, descending vertical motions occur where tropical SSTs are coolest, such as the eastern equatorial Pacific and western Indian Ocean where sub-surface waters upwell along the eastern margins of Africa and Arabia.

The emergence of the modern tropical Pacific zonal SST gradient that drives these large-scale tropical climate gradients occurred between 3 and 2 Ma based on multiple SST proxy records [109–112] and was broadly coeval with the transition towards drier and more open, C_4 -rich vegetation in East Africa [108,112]. Northern African aridity was found to be largely unaffected by the emergence of these zonal tropical SST gradients [108], providing a plausible mechanism for different vegetation histories of these two regions.

6. Conclusion

Our detailed $\delta^{13}C_{wax}$ and δD_{wax} analyses of two short (100 kyr) intervals at ODP Site 967 in the eastern Mediterranean basin documents large vegetation and hydroclimate cycles corresponding to orbital precession forcing of African monsoonal circulation and intensity. These intervals were selected for their nearly identical orbital eccentricity and precession amplitude configuration and because they bracket an important transition to more open East African vegetation between 3 and 2 Ma. The amplitude of $\delta^{13}C_{wax}$ cycles was 3–4‰, corresponding to 50–80% C_4 vegetation. The amplitude of δD_{wax} cycles was about 20–30‰, comparable with δD_{wax} records of the most recent African Humid Period (15–5 ka BP) from ocean and lake archives.

We find no significant difference in means or standard deviations of the $\delta^{13}C_{wax}$ and δD_{wax} values between the 3.05 and 1.75 Ma intervals, suggesting that vegetation and

hydroclimate responses to precessional monsoonal forcing were comparable for these two periods in the eastern Sahara domain. The lack of a significant increase in C_4 vegetation between these two intervals contrasts with the well-known increase in C_4 vegetation documented for many East African localities and in the Gulf of Aden [2,9,11].

Although further analysis of the Site 967 sediments would be required to confirm this finding, we tentatively conclude that the eastern Sahara dust source region (Algeria) did not experience the remarkable C_4 expansion in the East African domains of Kenya, Tanzania and Ethiopia. We propose that this East African C_4 grassland expansion between 3 and 2 Ma may have been a consequence of the coeval emergence of tropical ocean SST gradients at this time [109–112]. Climate model experiments constrained by palaeoceanographic observations have documented that the broad East African geographical domain would have become drier, and arid-adapted C_4 vegetation would have presumably increased, with the emergence of large zonal tropical SST gradients [108,112].

Our results also speak to a subtle, but important distinction noted in the Feakins *et al.* [11] Gulf of Aden study. Specifically, our results support their conclusion that orbital-scale palaeovegetation and palaeohydrologic variability can be as large, or larger, than long-term, secular shifts. Such observations conform to the very large orbital-scale palaeovegetation and palaeohydrologic variability detected at palaeolake Olduvai (*ca* 1.9–1.8 Ma [15,16]) and thus highlight the relative importance of shorter orbital-scale versus longer secular landscape remodelling influences on early hominin evolution in East Africa [17,113,114].

Data accessibility. All organic and isotopic geochemical data for this study have been uploaded as the electronic supplementary material. These data are also available through Interdisciplinary Earth Data Alliance (doi:10.1594/IEDA/100586).

Authors' contributions. P.B.d.M., C.R., J.E.T. and P.J.P. conceived the study and supervised the work. C.R., J.E.T., T.F. and P.J.P. acquired the data. All authors analysed and interpreted the data. C.R. and P.B.d.M. wrote the paper and C.R. drafted the figures with input and assistance from all co-authors.

Competing interests. We have no competing interests.

Funding. Funding for this study was provided by Columbia University's Center for Climate and Life and an NSF Graduate Research Fellowship to C.R.

Acknowledgements. We acknowledge Richard Leakey's support and encouragement of the next generation of Earth scientists pursuing human origins research questions. We thank Tim Herbert and one anonymous reviewer for their very helpful and thorough reviews that greatly improved the manuscript. We thank Robert Foley, Marta Lahr, Lawrence Martin and Chris Stringer for the opportunity to present this work and contribute this paper. We are grateful to the Ocean Drilling Program for providing the Site 967 samples. This is Lamont-Doherty Earth Observatory contribution no. 8004.

References

1. Bobe R, Behrensmeyer AK. 2004 The expansion of grassland ecosystems in Africa in relation to mammalian evolution and the origin of the genus *Homo*. *Palaeogeography* **207**, 399–420. (doi:10.1016/j.palaeo.2003.09.033)
2. Levin NE, Naomi E. 2015 Environment and climate of early human evolution. *Annu. Rev. Earth Planet. Sci.* **43**, 405–429. (doi:10.1146/annurev-earth-060614-105310)
3. deMenocal PB. 1995 Plio-Pleistocene African climate. *Science* **270**, 53–59. (doi:10.1126/science.270.5233.53)
4. Feakins SJ. 2013 Pollen-corrected leaf wax D/H reconstructions of northeast African hydrological changes during the late Miocene. *Palaeogeogr. Palaeoclim. Palaeoecol.* **374**, 1–10. (doi:10.1016/j.palaeo.2013.01.004)
5. Larrasoana JC, Roberts AP, Rohling EJ, Winkhofer M, Wehausen R. 2003 Three million years of monsoon variability over the northern Sahara. *Clim. Dyn.* **21**, 689–698. (doi:10.1007/s00382-003-0355-z)

6. Tierney JE, Russell JM, Huang Y. 2010 A molecular perspective on Late Quaternary climate and vegetation change in the Lake Tanganyika basin, East Africa. *Quat. Sci. Rev.* **29**, 787–800. (doi:10.1016/j.quascirev.2009.11.030)
7. Wynn JG. 2004 Influence of Plio-Pleistocene aridification on human evolution: evidence from paleosols of the Turkana Basin, Kenya. *Am. J. Phys. Anthropol.* **123**, 106–118. (doi:10.1002/ajpa.10317)
8. National Research Council 2010 *Understanding climate's influence on human evolution*. Washington, DC: National Academies Press.
9. Cerling TE *et al.* 2011 Woody cover and hominin environments in the past 6 million years. *Nature* **476**, 51–56. (doi:10.1038/nature10306)
10. Levin NE, Brown FH, Behrensmeyer AK, Bobe R, Cerling TE. 2011 Paleosol carbonates from the Omo Group: isotopic records of local and regional environmental change in East Africa. *Palaeogeogr. Palaeoclim. Palaeoecol.* **307**, 75–89. (doi:10.1016/j.palaeo.2011.04.026)
11. Feakins SJ, deMenocal PB, Eglinton TI. 2005 Biomarker records of Late Neogene changes in northeast African vegetation. *Geology* **33**, 977. (doi:10.1130/G21814.1)
12. Feakins SJ, Levin NE, Liddy HM, Sieracki A, Eglinton TI, Bonnefille R. 2013 Northeast African vegetation change over 12 m.y. *Geology* **41**, 295–298. (doi:10.1130/G33845.1)
13. Garcin Y, Melnick D, Strecker MR, Olago D, Tiercelin J-J. 2012 East African mid-Holocene wet–dry transition recorded in palaeo-shorelines of Lake Turkana, northern Kenya Rift. *Earth Planet. Sci. Lett.* **331–332**, 322–334. (doi:10.1016/j.epsl.2012.03.016)
14. Larrasoana JC, Roberts AP, Rohling EJ. 2013 Dynamics of Green Sahara Periods and their role in hominin evolution. *PLoS ONE* **8**, e76514. (doi:10.1371/journal.pone.0076514)
15. Magill CR, Ashley GM, Freeman KH. 2012 Ecosystem variability and early human habitats in eastern Africa. *Proc. Natl Acad. Sci. USA* **110**, 1167–1174. (doi:10.1073/pnas.1206276110)
16. Magill CR, Ashley GM, Freeman KH. 2012 Water, plants, and early human habitats in eastern Africa. *Proc. Natl Acad. Sci. USA* **110**, 1175–1180. (doi:10.1073/pnas.1209405109)
17. Potts R, Faith JT. 2015 Alternating high and low climate variability: the context of natural selection and speciation in Plio-Pleistocene hominin evolution. *J. Hum. Evol.* **87**, 5–20. (doi:10.1016/j.jhevol.2015.06.014)
18. deMenocal PB. 2004 African climate change and faunal evolution during the Pliocene–Pleistocene. *Earth Planet. Sci. Lett.* **220**, 3–24. (doi:10.1016/S0012-821X(04)00003-2)
19. Trauth MH, Maslin MA, Deino A, Strecker MR. 2005 Late Cenozoic moisture history of East Africa. *Science* **1**, 1126. (doi:10.1126-Science.1112964)
20. Laskar J, Robutel P, Joutel F, Gastineau M, Correia A, Levrard B. 2004 A long-term numerical solution for the insolation quantities of the Earth. *Astron. Astrophys.* **428**, 261–285. (doi:10.1051/0004-6361:20041335)
21. Lourens LJ, Antonarakou A, Hilgen FJ, Van Hoof A, vergaud-Grazzini C, Zachariasse WJ. 1996 Evaluation of the Plio-Pleistocene astronomical timescale. *Paleoceanography* **11**, 391–413. (doi:10.1029/96PA01125)
22. Kroon D, Alexander I, Little M, Lourens LJ, Mattewson A, Roberston AHF, Sakamoto T. 1998 Oxygen isotope and sapropel stratigraphy in the eastern Mediterranean during the last 3.2 Ma. In *Proc. ODP Sci. Res.* (eds AHF Roberston, KC Emeis, C Richter, A Camerlenghi), pp. 181–189. College Station, TX: ODP.
23. White F. 1983 *The vegetation of Africa, a descriptive memoir to accompany the UNESCO/AETFAT/UNSO vegetation map of Africa (3 plates, Northwestern Africa, Northeastern Africa, and Southern Africa, 1: 5,000,000)*. Paris, France: UNESCO.
24. Nicholson SE. 2000 The nature of rainfall variability over Africa on time scales of decades to millennia. *Glob. Planet. Change* **26**, 137–158. (doi:10.1016/S0921-8181(00)00040-0)
25. Goudie AS, Middleton NJ. 2001 Saharan dust storms: nature and consequences. *Earth Sci. Rev.* **56**, 179–204. (doi:10.1016/S0012-8252(01)00067-8)
26. Ganor E, Mamane Y. 1982 Transport of Saharan dust across the eastern Mediterranean. *Atmos. Environ.* (1967) **16**, 581–587. (doi:10.1016/0004-6981(82)90167-6)
27. Kutzbach JE. 1981 Monsoon climate of the early Holocene: climate experiment with the earth's orbital parameters for 9000 years ago. *Science* **214**, 59–61. (doi:10.1126/science.214.4516.59)
28. McGee D, deMenocal PB, Winckler G, Stuut JBW, Bradtmiller LI. 2013 The magnitude, timing and abruptness of changes in North African dust deposition over the last 20 000 yr. *Earth Planet. Sci. Lett.* **371–372**, 163–176. (doi:10.1016/j.epsl.2013.03.054)
29. Tierney JE, deMenocal PB. 2013 Abrupt shifts in Horn of Africa hydroclimate since the last glacial maximum. *Science* **342**, 843–846. (doi:10.1126/science.1240411)
30. Skonieczny C *et al.* 2015 African humid periods triggered the reactivation of a large river system in western Sahara. *Nat. Commun.* **6**, 8751. (doi:10.1038/ncomms9751)
31. deMenocal PB, Tierney JE. 2012 African humid periods paced by Earth's orbital changes. *Nat. Educ.* **3**, 12.
32. Rohling EJ, Marino G, Grant KM. 2015 Earth-science reviews. *Earth Sci. Rev.* **143**, 62–97. (doi:10.1016/j.earscirev.2015.01.008)
33. Hilgen F. 1991 Astronomical calibration of Gauss to Matuyama sapropels in the Mediterranean and implication for the geomagnetic polarity time scale. *Earth Planet. Sci. Lett.* **104**, 226–244. (doi:10.1016/0012-821X(91)90206-W)
34. Rossignol-Strick M. 1983 African monsoons, an immediate climate response to orbital insolation. *Nature* **303**, 46–49. (doi:10.1038/304046a0)
35. Sachs JP, Repeta DJ. 1999 Oligotrophy and nitrogen fixation during eastern Mediterranean sapropel events. *Science* **286**, 2485–2488. (doi:10.1126/science.286.5449.2485)
36. Pachur H-J, Kröpelin S. 1987 Wadi Howar: paleoclimatic evidence from an extinct river system in the southeastern Sahara. *Science* **237**, 298–300. (doi:10.1126/science.237.4812.298)
37. Rohling E *et al.* 2002 African monsoon variability during the previous interglacial maximum. *Earth Planet. Sci. Lett.* **202**, 61–75. (doi:10.1016/S0012-821X(02)00775-6)
38. Emeis KC *et al.* 2003 Eastern Mediterranean surface water temperatures and $\delta^{18}\text{O}$ composition during deposition of sapropels in the late Quaternary. *Paleoceanography* **18**, PA1005. (doi:10.1029/2000PA000617)
39. Paillou P, Schuster M, Tooth S, Farr T, Rosenqvist A, Lopez S, Malezieux J-M. 2009 Mapping of a major paleodrainage system in eastern Libya using orbital imaging radar: the Kufrah River. *Earth Planet. Sci. Lett.* **277**, 327–333. (doi:10.1016/j.epsl.2008.10.029)
40. Sakamoto T, Janacek T, Emeis KC. 1998 Continuous sedimentary sequences from the eastern Mediterranean Sea: composite depth sections. *Proc. ODP, Sci. Results* **160**, 37–59. College Station, TX: Ocean Drilling Program. (doi:10.2973/odp.proc.sr.160.053.1998)
41. Wehausen R, Brumsack HJ. 2000 Chemical cycles in Pliocene sapropel-bearing and sapropel-barren eastern Mediterranean sediments. *Palaeogeogr. Palaeoclim. Palaeoecol.* **158**, 325–352. (doi:10.1016/S0031-0182(00)00057-2)
42. Brumsack HJ, Wehausen R. 1999 A geochemical record of precession-induced cyclic eastern Mediterranean sedimentation: implications for northern Sahara humidity during the Pliocene. *Naturwissenschaften* **86**, 281–286. (doi:10.1007/S001140050615)
43. Joordens JCA, Vonhof HB, Feibel CS, Lourens LJ, Dupont-Nivet G, van der Lubbe JHJL, Sier MJ, Davies GR, Kroon D. 2011 An astronomically-tuned climate framework for hominins in the Turkana Basin. *Earth Planet. Sci. Lett.* **307**, 1–8. (doi:10.1016/j.epsl.2011.05.005)
44. Tierney JE, Russell JM, Huang Y, Damste JSS, Hopmans EC, Cohen AS. 2008 Northern Hemisphere controls on tropical southeast African climate during the past 60 000 years. *Science* **322**, 252–255. (doi:10.1126/science.1160485)
45. Tierney JE, Lewis SC, Cook BI, LeGrande AN, Schmidt GA. 2011 Model, proxy and isotopic perspectives on the East African humid period. *Earth Planet. Sci. Lett.* **307**, 103–112. (doi:10.1016/j.epsl.2011.04.038)
46. Bobe R, Behrensmeyer AK, Chapman RE. 2002 Faunal change, environmental variability and late Pliocene hominin evolution. *J. Hum. Evol.* **42**, 475–497. (doi:10.1006/jhevol.2001.0535)
47. Cerling TE, Harris JM, MacFadden BJ, Leakey MG, Quade J, Eisenmann V, Ehleringer JR. 1997

- Global vegetation change through the Miocene/Pliocene boundary. *Nature* **389**, 153–158. (doi:10.1038/38229)
48. Uno KT, Cerling TE, Harris JM, Kunimatsu Y, Leakey MG, Nakatsukasa M, Nakaya H. 2011 Late Miocene to Pliocene carbon isotope record of differential diet change among East African herbivores. *Proc. Natl Acad. Sci. USA* **108**, 6509–6514. (doi:10.1073/pnas.1018435108)
49. Bonnefille R. 2010 Cenozoic vegetation, climate changes and hominid evolution in tropical Africa. *Glob. Planet. Change* **72**, 390–411. (doi:10.1016/j.gloplacha.2010.01.015)
50. Cerling TE, Bowman JR, O'Neil JR. 1988 An isotopic study of a fluvial-lacustrine sequence: the Plio-Pleistocene Koobi Fora sequence, East Africa. *Palaeogeogr. Palaeoclim. Palaeoecol.* **63**, 335–356. (doi:10.1016/0031-0182(88)90104-6)
51. Emeis KC, Sakamoto T, Wehausen R, Brumsack HJ. 2000 The sapropel record of the eastern Mediterranean Sea—results of Ocean Drilling Program Leg 160. *Palaeogeogr. Palaeoclim. Palaeoecol.* **158**, 371–395. (doi:10.1016/S0031-0182(00)00059-6)
52. Herbert TD, Ng G, Peterson LC. 2015 Evolution of Mediterranean sea surface temperatures 3.5–1.5 Ma: regional and hemispheric influences. *Earth Planet. Sci. Lett.* **409**, 307–318. (doi:10.1016/j.epsl.2014.10.006)
53. Emeis KC, Schulz HM, Struck U, Sakamoto T, Doose H, Erlenkeuser H, Howell M, Kroon D, Paterne M. 1998 Stable isotope and alkenone temperature records of sapropels from sites 964 and 967: constraining the physical environment of sapropel formation in the eastern Mediterranean Sea. *Proc. ODP, Sci. Results* **160**, 309–331. College Station, TX: Ocean Drilling Program. (doi:10.2973/odp.proc.sr.160.011.1998)
54. van der Meer M, Baas M, Rijpstra WIC. 2007 Hydrogen isotopic compositions of long-chain alkenones record freshwater flooding of the eastern Mediterranean at the onset of sapropel deposition. *Earth Planet. Sci. Lett.* **262**, 594–600. (doi:10.1016/j.epsl.2007.08.014)
55. Thunell RC, Williams DF. 1989 Glacial-Holocene salinity changes in the Mediterranean Sea: hydrographic and depositional effects. *Nature* **338**, 493–496. (doi:10.1038/338493a0)
56. Schefuss E. 2003 Carbon isotope analyses of n-alkanes in dust from the lower atmosphere over the central eastern Atlantic. *Geochim. Cosmochim. Acta* **67**, 1757–1767. (doi:10.1016/S0016-7037(02)01414-X)
57. Furbank RT, Taylor WC. 1995 Regulation of photosynthesis in C3 and C4 plants: a molecular approach. *Plant Cell* **7**, 797.
58. Sage RF. 2004 The evolution of C4 photosynthesis. *New Phytol.* **161**, 341–370. (doi:10.1046/j.1469-8137.2004.00974.x)
59. Eglinton G, Hamilton RJ. 1967 Leaf epicuticular waxes. *Science* **156**, 1322–1335. (doi:10.1126/science.156.3780.1322)
60. Sachse D, Radke J, Gleixner G. 2004 Hydrogen isotope ratios of recent lacustrine sedimentary n-alkanes record modern climate variability. *Geochim. Cosmochim. Acta* **63**, 4877–4889. (doi:10.1016/j.gca.2004.06.004)
61. Huang Y, Dupont L, Sarnthein M, Hayes JM, Eglinton G. 2000 Mapping of C4 plant input from North West Africa into North East Atlantic sediments. *Geochim. Cosmochim. Acta* **64**, 3505–3513. (doi:10.1016/S0016-7037(00)00445-2)
62. Schefuss E, Schouten S, Jansen JHF, Damste JSS. 2003 African vegetation controlled by tropical sea surface temperatures in the mid-Pleistocene period. *Nature* **422**, 418–421. (doi:10.1038/nature01500)
63. Brooks JD, Smith JW. 1967 The diagenesis of plant lipids during the formation of coal, petroleum and natural gas. I. Changes in the n-paraffin hydrocarbons. *Geochim. Cosmochim. Acta* **31**, 2389–2397. (doi:10.1016/0016-7037(67)90010-5)
64. Sachse D *et al.* 2012 Molecular paleohydrology: interpreting the hydrogen-isotopic composition of lipid biomarkers from photosynthesizing organisms. *Ann. Rev. Earth Planet. Sci.* **40**, 221–249. (doi:10.1146/annurev-earth-042711-105535)
65. Hou J, D'Andrea WJ, Huang Y. 2008 Can sedimentary leaf waxes record D/H ratios of continental precipitation? Field, model and experimental assessments. *Geochim. Cosmochim. Acta* **72**, 3503–3517. (doi:10.1016/j.gca.2008.04.030)
66. Eglinton TI, Eglinton G. 2008 Molecular proxies for paleoclimatology. *Earth Planet. Sci. Lett.* **275**, 1–16. (doi:10.1016/j.epsl.2008.07.012)
67. Garcin Y, Schwab VF, Gleixner G, Kahmen A, Todou G, Séné O, Onana J-M, Achoundong G, Sachse D. 2012 Hydrogen isotope ratios of lacustrine sedimentary n-alkanes as proxies of tropical African hydrology: insights from a calibration transect across Cameroon. *Geochim. Cosmochim. Acta* **79**, 106–126. (doi:10.1016/j.gca.2011.11.039)
68. Dansgaard W. 1964 Stable isotopes in precipitation. *Tellus* **16**, 436–468. (doi:10.1111/j.2153-3490.1964.tb00181.x)
69. Tierney JE, Smerdon JE, Anchukaitis KJ, Seager R. 2013 Multidecadal variability in East African hydroclimate controlled by the Indian Ocean. *Nature* **493**, 389–392. (doi:10.1038/nature11785)
70. Hedges JL, Mann DC. 1979 The characterization of plant tissues by their lignin oxidation products. *Geochim. Cosmochim. Acta* **43**, 1803–1807. (doi:10.1016/0016-7037(79)90028-0)
71. Meyers PA, Ishiwatari R. 1993 Lacustrine organic geochemistry—an overview of indicators of organic matter sources and diagenesis in lake sediments. *Org. Geochem.* **20**, 867–900. (doi:10.1016/0146-6380(93)90100-P)
72. Filley TR, Freeman KH, Bianchi TS, Baskaran M. 2001 An isotopic biogeochemical assessment of shifts in organic matter input to Holocene sediments from Mud Lake, Florida. *Org. Geochem.* **32**, 1153–1167. (doi:10.1016/S0146-6380(01)00063-8)
73. Krom MD, Michard A, Cliff RA, Strohle K. 1999 Sources of sediment to the Ionian Sea and western Levantine basin of the eastern Mediterranean during S-1 sapropel times. *Mar. Geol.* **160**, 45–61. (doi:10.1016/S0025-3227(99)00015-8)
74. Polissar PJ, D'Andrea WJ. 2014 Uncertainty in paleohydrologic reconstructions from molecular δD values. *Geochim. Cosmochim. Acta* **129**, 146–156. (doi:10.1016/j.gca.2013.12.021)
75. Sauer PE, Eglinton TI, Hayes JM, Schimmelmann A, Sessions AL. 2001 Compound-specific D/H ratios of lipid biomarkers from sediments as a proxy for environmental and climatic conditions. *Geochim. Cosmochim. Acta* **65**, 213–222. (doi:10.1016/S0016-7037(00)00520-2)
76. Lisiecki LE. 2005 A Pliocene-Pleistocene stack of 57 globally distributed benthic $\delta^{18}O$ records. *Paleoceanography* **20**, PA1003. (doi:10.1029/2004PA001071)
77. Schrag DP, Hampt G, Murray DW. 1996 Pore fluid constraints on the temperature and oxygen isotopic composition of the glacial ocean. *Science* **272**, 1930–1932. (doi:10.1126/science.272.5270.1930)
78. Gat J. 1996 Oxygen and hydrogen isotopes in the hydrologic cycle. *Annu. Rev. Earth Planet. Sci.* **24**, 225–262. (doi:10.1146/annurev.earth.24.1.225)
79. Tipple BJ, Meyers SR, Pagani M. 2010 Carbon isotope ratio of Cenozoic CO_2 : a comparative evaluation of available geochemical proxies. *Paleoceanography* **25**, PA3202. (doi:10.1029/2009PA001851)
80. Farquhar GD, Ehleringer JR, Hubick KT. 1989 Carbon isotope discrimination and photosynthesis. *Annu. Rev. Plant Physiol. Plant Mol. Biol.* **40**, 503–537. (doi:10.1146/annurev.pp.40.060189.002443)
81. Dalzell BJ, Filley TR, Harbor JM. 2005 Flood pulse influences on terrestrial organic matter export from an agricultural watershed. *J. Geophys. Res.* **110**, G02011. (doi:10.1029/2005JG000043)
82. Chikaraishi Y, Naraoka H, Poulson SR. 2004 Carbon and hydrogen isotopic fractionation during lipid biosynthesis in a higher plant (*Cryptomeria japonica*). *Phytochemistry* **65**, 323–330. (doi:10.1016/j.phytochem.2003.12.003)
83. Chikaraishi Y, Naraoka H, Poulson SR. 2004 Hydrogen and carbon isotopic fractionations of lipid biosynthesis among terrestrial (C3, C4 and CAM) and aquatic plants. *Phytochemistry* **65**, 1369–1381. (doi:10.1016/j.phytochem.2004.03.036)
84. Collister JW, Rieley G, Stern B, Eglinton G, Fry B. 1994 Compound-specific $\delta^{13}C$ analyses of leaf lipids from plants with differing carbon dioxide metabolisms. *Org. Geochem.* **21**, 619–627.
85. Vogts A, Moossen H, Rommerskirchen F, Rullkötter J. 2009 Distribution patterns and stable carbon isotopic composition of alkanes and alkan-1-ols from plant waxes of African rain forest and savanna C3 species. *Org. Geochem.* **40**, 1037–1054. (doi:10.1016/j.orggeochem.2009.07.011)
86. Francey RJ, Allison CE, Etheridge DM, Trudinger CM, Enting IG, Leuenberger M, Langenfelds RL, Michel

- E, Steele LP. 1999 A 1000-year high precision record of $\delta^{13}\text{C}$ in atmospheric CO_2 . *Tellus* **51B**, 170–193. (doi:10.1034/j.1600-0889.1999.t01-1-00005.x)
87. Keeling CD, Piper SC, Bacastow RB, Wahlen M, Whorf TP, Heimann M, Meijer HA. 2005 Atmospheric CO_2 and ^{13}C exchange with the terrestrial biosphere and oceans from 1978 to 2000: observations and carbon cycle implications. In *A history of atmospheric CO_2 and its effects on plants, animals, and ecosystems* (eds IT Baldwin *et al.*), pp. 83–113. New York, NY: Springer.
88. Magill CR, Ashley GM, Freeman KH. 2013 Water, plants, and early human habitats in eastern Africa. *Proc. Natl Acad. Sci. USA* **110**, 1175–1180. (doi:10.1073/pnas.1209405109)
89. Rossignol-Strick M. 1985 Mediterranean Quaternary sapropels, an immediate response of the African monsoon to variation of insolation. *Palaeogeogr. Palaeoclim. Palaeoecol.* **49**, 237–263. (doi:10.1016/0031-0182(85)90056-2)
90. Wehausen R, Brumsack HJ. 2002 Astronomical forcing of the East Asian monsoon mirrored by the composition of Pliocene South China Sea sediments. *Earth Planet. Sci. Lett.* **201**, 621–636. (doi:10.1016/S0012-821X(02)00746-X)
91. Kroepelin S *et al.* 2008 Climate-driven ecosystem succession in the Sahara: the past 6000 years. *Science* **320**, 765–768. (doi:10.1126/science.1154913)
92. Menzel D, Schouten S, van Bergen PF, Damsté JSS. 2004 Higher plant vegetation changes during Pliocene sapropel formation. *Org. Geochem.* **35**, 1343–1353. (doi:10.1016/j.orggeochem.2004.02.011)
93. Schefuß E, Schouten S, Schneider RR. 2005 Climatic controls on central African hydrology during the past 20 000 years. *Nature* **437**, 1003–1006. (doi:10.1038/nature03945)
94. Shipboard Scientific Party 1996 ODP Leg 160, Site 967. *Proc. ODP, Init. Repts* **160**, 215–287. College Station, TX: Ocean Drilling Program. (doi:10.2973/odp.proc.ir.160.108.1996)
95. Raymo ME, Lisiecki LE, Nisancioglu KH. 2006 Pliocene-pleistocene ice volume, Antarctic climate, and the global delta O-18 record. *Science* **313**, 492–495. (doi:10.1126/science.1123296)
96. Wehausen R, Brumsack HJ. 1999 Cyclic variations in the chemical composition of eastern Mediterranean Pliocene sediments: a key for understanding sapropel formation. *Mar. Geol.* **153**, 161–176. (doi:10.1016/S0025-3227(98)00083-8)
97. Galy V, Eglinton T, France-Lanord C, Sylva S. 2011 The provenance of vegetation and environmental signatures encoded in vascular plant biomarkers carried by the Ganges–Brahmaputra rivers. *Earth Planet. Sci. Lett.* **304**, 1–12. (doi:10.1016/j.epsl.2011.02.003)
98. Jolly D *et al.* 1998 Biome reconstruction from pollen and plant macrofossil data for Africa and the Arabian peninsula at 0 and 6000 years. *J. Biogeogr.* **25**, 1007–1027. (doi:10.1046/j.1365-2699.1998.00238.x)
99. Hoelzmann P, Jolly D, Harrison SP, Laarif F, Bonnefille R, Pachur H-J. 1998 Mid-Holocene land-surface conditions in northern Africa and the Arabian Peninsula: a data set for the analysis of biogeophysical feedbacks in the climate system. *Glob. Biogeochem. Cycles* **12**, 35–51. (doi:10.1029/97GB02733)
100. Lezine A-M, Hély C, Grenier C, Braconnot P, Krinner G. 2011 Sahara and Sahel vulnerability to climate changes: lessons from Holocene hydrological data. *Quat. Sci. Rev.* **30**, 3001–3012. (doi:10.1016/j.quascirev.2011.07.006)
101. Lezine A-M, Zheng W, Braconnot P, Krinner G. 2011 Late Holocene plant and climate evolution at Lake Yoah, northern Chad: pollen data and climate simulations. *Clim. Past* **7**, 1351–1362. (doi:10.5194/cp-7-1351-2011-supplement)
102. Pearcy RW, Ehleringer J. 1984 Comparative ecophysiology of C3 and C4 plants. *Plant Cell Environ.* **7**, 1–13. (doi:10.1111/j.1365-3040.1984.tb01194.x)
103. Collins JA, Schefuß E, Mulitza S, Prange M, Werner M, Tharammal T, Paul A, Wefer G. 2013 Estimating the hydrogen isotopic composition of past precipitation using leaf-waxes from western Africa. *Quat. Sci. Rev.* **65**, 88–101. (doi:10.1016/j.quascirev.2013.01.007)
104. Lisiecki LE, Raymo ME. 2005 A Pliocene-Pleistocene stack of 57 globally distributed benthic $\delta^{18}\text{O}$ records. *Paleoceanography* **20**, PA1003. (doi:10.1029-2004PA001071)
105. Foucault A, Stanley DJ. 1989 Late Quaternary palaeoclimatic oscillations in East Africa recorded by heavy minerals in the Nile delta. *Nature* **339**, 44–46. (doi:10.1038/339044a0)
106. Bibi F, Kiessling W. 2015 Continuous evolutionary change in Plio-Pleistocene mammals of eastern Africa. *Proc. Natl Acad. Sci. USA* **112**, 10 623–10 628. (doi:10.1073/pnas.1504538112/-/DCSupplemental/pnas.201504538SI.pdf)
107. Philander S, Fedorov A. 2003 Role of tropics in changing the response to Milankovitch forcing some three million years ago. *Paleoceanography* **18**, 1045. (doi:10.1029/2002PA000837)
108. Brierley CM, Fedorov AV. 2010 Relative importance of meridional and zonal sea surface temperature gradients for the onset of the ice ages and Pliocene-Pleistocene climate evolution. *Paleoceanography* **25**, PA2214. (doi:10.1029/2009PA001809)
109. Wara MW, Ravelo AC, Delaney ML. 2005 Permanent El Niño-like conditions during the Pliocene warm period. *Science* **309**, 758–761. (doi:10.1126/science.1114760)
110. Ravelo AC, Lawrence KT, Fedorov A, Ford HL. 2014 Comment on ‘a 12-million-year temperature history of the tropical Pacific Ocean’. *Science* **346**, 1467–1467. (doi:10.1126/science.1257618)
111. Dekens PS, Ravelo AC, McCarthy MD. 2007 Warm upwelling regions in the Pliocene warm period. *Paleoceanography* **22**, PA3211. (doi:10.1029/2006PA001394)
112. Brierley CM, Fedorov AV, Liu Z, Herbert TD, Lawrence KT, LaRiviere JP. 2009 Greatly expanded tropical warm pool and weakened Hadley circulation in the Early Pliocene. *Science* **323**, 1714–1718. (doi:10.1126/science.1167625)
113. Antón SC, Potts R, Aiello L. 2014 Evolution of early *Homo*: an integrated biological perspective. *Science* **345**, 1–15. (doi:10.1126/science.1236828)
114. deMenocal PB. 2011 Climate and human evolution. *Science* **331**, 540–542. (doi:10.1126/science.1190683)